Measurement of the Liquid Film Thickness in Micro Tube Slug Flow

Youngbae Han and Naoki Shikazono

Department of Mechanical Engineering, The University of Tokyo

Hongo 7-3-1, Bunkyo-ku, Tokyo, 113-8656, Japan

Tel: +81-3-5841-6419; Fax: +81-3-5800-6999.

Abstract

Slug flow is one of the representative flow regimes of two-phase flow in micro tubes. It is well known that the thin liquid film formed between the tube wall and the vapor bubble plays an important role in micro tube heat transfer. In the present study, experiments are carried out to clarify the effects of parameters that affect the formation of the thin liquid film in micro tube two-phase flow. Laser focus displacement meter is used to measure the thickness of the thin liquid film. Air, ethanol, water and FC-40 are used as working fluids. Circular tubes with five different diameters, $D = 0.3$, 0.5, 0.7, 1.0 and 1.3 mm, are used. It is confirmed that the liquid film thickness is determined only by capillary number and the effect of inertia force is negligible at small capillary numbers. However, the effect of inertia force cannot be neglected as capillary number increases. At relatively high capillary numbers, liquid film thickness takes a minimum value against Reynolds number. The effects of bubble length, liquid slug length and gravity on the liquid film thickness are also investigated. Experimental correlation for the initial liquid film thickness based on capillary number, Reynolds number and Weber number is proposed.

Key words: Two-phase flow, Micro tube, Liquid film thickness, Slug flow

Nomenclature

Bo Bond number, $Bo = \rho g D^2/\sigma$

Ca capillary number, $Ca = \mu U/\sigma$

D tube diameter, [m]

g acceleration of gravity, [m/s^2]

L length, [m]

n refractive index

Re Reynolds number, $Re = \rho U D/\mu$

T temperature, [°C]

U velocity, [m/s]

We Weber number, $We = \rho U^2 D/\sigma$

y_{m} distance of objective lens movement, [m]

Greek Symbols

α angle of the cover glass [radian]

Email addresses: ybhan@feslab.t.u-tokyo.ac.jp (Youngbae Han), shika@feslab.t.u-tokyo.ac.jp (Naoki Shikazono).

δ liquid film thickness, [m]

κ curvature of the bubble nose, [1/m]

λ length of the transition region, [m]

μ viscosity, [Pa·s]

ρ density, [kg/m^3]

σ surface tension, [N/m]

θ angle of incidence or refraction, [radian]

Subscripts

0	initial
1	through Z axis in Fig. 5
2	through X axis in Fig. 5
actuator	actuator
bottom	tube bottom in horizontal flow direction
bubble	bubble
f	fluid
side	tube side in horizontal flow direction
slug	liquid slug

w wall

1 Introduction

Micro scale heat transfer attracts large attention due to its many advantages, e.g., high efficiency, miniaturization, etc. However, the characteristics of two-phase flow in micro tubes are quite different from those in conventional tubes and they are not fully understood. Flow regimes are also different in micro tubes due to surface tension, and slug flow becomes one of the dominant flow patterns. It is known that the thin liquid film formed between the tube wall and the vapor bubble plays an important role in micro tube heat transfer. It is reported that the liquid film thickness is one of the important parameters for the prediction of flow boiling heat transfer in micro tubes (Thome et al., 2004; Kenning et al., 2006).

Many researches on the liquid film thickness in slug flow have been conducted both experimentally and theoretically. Taylor (1961) experimentally obtained the mean liquid film thickness remaining on the wall by measuring the difference of the bubble velocity and the mean velocity. Highly viscous fluids, i.e., glycerine, syrup-water mixture and lubricating oil, were used and thus wide capillary number range was covered. It is reported that the liquid film thickness increases with capillary number and reaches a certain fraction of the tube diameter. Bretherton (1961) suggested an analytical theory on the liquid film thickness and axial pressure drop across the bubble with the lubrication equations. Assuming small capillary number, it is shown that the dimensionless liquid film thickness can be scaled with $Ca^{2/3}$.

Moriyama et al. (1996) obtained the liquid film thickness formed by a vapor bubble expansion in a narrow gap by measuring the temperature change of the channel wall, which was initially superheated. In their experiment, it was assumed that whole liquid film on the wall evaporates and the heat is consumed by the evaporation of the liquid film. Their experimental data was correlated in terms of capillary number and Bond number based on the interface acceleration. Heil (2001) investigated the effect of inertial force on the liquid film thickness numerically. It is shown that the liquid film thickness and the pressure gradient are dependent on the Reynolds number.

Aussillous and Quere (2000) measured the liquid film thickness using fluids with relatively low surface tension. It was found that the liquid film thickness deviates from the Taylor's data at relatively high capillary numbers. Visco-inertia regime where the effect of inertial force on the liquid film thickness becomes significant was demonstrated. Kreutzer et al. (2005) investigated the liquid film thickness and the pressure drop in a micro tube both numerically and experimentally. Predicted liquid film thickness showed almost the same trend with that reported by Heil (2001).

Utaka et al. (2007) measured the liquid film thickness formed by a vapor bubble in a narrow gap mini-channel with laser extinction method and investigated the heat transfer characteristics quantitatively. It is concluded that the boiling phenomena are determined by two kinds of characteristic periods, i.e., the micro-layer dominant and the liquid saturated periods.

Although many experiments have been carried out to measure the liquid film thickness in micro tubes, quantitative data of local and instantaneous liquid film thicknesses are still limited. To develop a precise heat transfer model in a

micro tube, it is crucial to know the characteristics of the liquid film thickness. In the present study, local and instantaneous liquid film thicknesses are measured directly with laser focus displacement meter. Series of experiments is conducted to investigate the effects of capillary number and Reynolds number on the formation of liquid film in micro tubes.

2 Experimental setup and procedure

2.1 Experimental setup

Figure 1 shows the schematic diagram of the experimental setup. Circular Pyrex glass tubes with inner diameters of 0.3, 0.5, 0.7, 1.0 and 1.3 mm were used as test tubes. Tube diameter was measured with a microscope and the averaged value of inlet and outlet inner diameters was used. Table 1 and Fig. 2 show the dimensions and the photograph of 0.487 mm inner diameter tube. The differences of inlet and outlet inner diameters are less than 1% for all tubes. One edge of Pyrex glass tube was connected to the syringe. Actuator motor (EZHC6A-101, Oriental motor) was used to control the velocity of liquid in the micro tube. The velocity range of the actuator motor is from 0 to 0.2 m/s. Syringes with several cross sectional areas were used to control the liquid velocity in the test section. The range of liquid velocity in the present experiment was varied from 0 to 7 m/s. The velocity of gas-liquid interface was measured from the images captured by the high speed camera (Phantom 7.1). Images were taken at several frame rates according to bubble velocity. For the maximum bubble velocity, frame rate was 10000 frames per second with a shutter time of 10 μs. Laser focus displacement meter (LT9010M, Keyence)

was used to measure the liquid film thickness. Laser focus displacement meter has been used by several researchers for the measurement of the liquid film thickness (Takamasa and Kobayashi, 2000; Hazuku et al., 2005). It is reported that the laser focus displacement meter can measure the liquid film thickness very accurately within 1% error (Hazuku et al., 2005). Figure 3 shows the principle of the laser focus displacement meter. The position of the target surface can be determined by the displacement of objective lens moved by the tuning fork. The intensity of the reflected light becomes highest in the light-receiving element when the focus is obtained on the target surface. Objective lens is vibrated continually in the range of ±0.3 mm. Liquid film thickness is obtained from those values. The resolution for the present laser focus displacement meter is 0.01 μm, the laser spot diameter is 2 μm and the response time is 640 μs. Measured liquid film thickness is transformed to DC voltage signal in the range of ±10 V. Output signal was sent to PC through GPIB interface and recorded with LabVIEW.

2.2 Correction for wall curvature

As the laser beam passes through the tube wall, focus is scattered within a certain range due to the difference of curvatures between axial and azimuthal directions. Cover glass and glycerol were used to remove the curvature effect caused by the outer wall as shown in Fig. 4. Refractive index of glycerol (n = 1.47) is almost the same with that of the Pyrex glass (n = 1.474), thus the refraction of laser between glycerol and Pyrex glass can be neglected. Refractive indices of ethanol, water and FC-40 are 1.36, 1.33 and 1.29. It is difficult to detect the interface between inner wall and liquid, because the

difference of the refractive indices of the Pyrex glass and the liquid is small. Therefore, the distance from the cover glass to the dry inner wall is initially measured without flowing the liquid. Then, the thickness with liquid film is measured. The liquid film thickness is calculated from the difference of these two values.

The effect of inner wall curvature is corrected by the equation suggested by Takamasa and Kobayashi (2000). Figure 5 shows the laser path and refraction through the liquid film. Focus is scattered from δ_1 to δ_2 due to the difference of wall curvatures in X and Z directions, respectively. Liquid film thickness is considered to be the average of δ_1 and δ_2, because the intensity of reflection may become highest at the center of δ_1 and δ_2. Liquid film thickness δ is obtained as follows:

$$\delta = \frac{\delta_1 + \delta_2}{2}. \tag{1}$$

In Eq. (1), δ_1 and δ_2 are the liquid film thicknesses through Z and X axes, respectively. Liquid film thickness δ_1 through Z axis can be calculated from Eqs. (2) and (3) as:

$$\delta_1 = y_{\mathrm{m}} \cdot \frac{\tan\theta_{\mathrm{w}}}{\tan\theta_{\mathrm{f}}}, \tag{2}$$

$$\frac{\sin\theta_{\mathrm{w}}}{\sin\theta_{\mathrm{f}}} = \frac{n_{\mathrm{f}}}{n_{\mathrm{w}}}, \tag{3}$$

where n_{f} and n_{w} are the refractive indices of the working fluid and the tube wall, respectively. In Eq. (2), y_{m} is the difference of the distance from the cover glass to the dry inner wall and the thickness with liquid film. y_m can be obtained as the distance of objective lens movement from the recorded data during the experiments. The angle of incidence θ_{w} is 10.07° in the present

laser focus displacement meter. The angle of refraction θ_{f} is determined from the Snellius's law as Eq. (3). Liquid film thickness δ_2 through X axis can be calculated from Eq. (4) as:

$$\delta_2 = y_0 + \frac{x_0}{\tan(\theta_{\mathrm{w}} - \theta'_{\mathrm{w}} + \theta'_{\mathrm{f}})}, \tag{4}$$

where θ'_w and θ'_f are the angle of incidence and the angle of refraction in X axis, and (x_0, y_0) is the intersection point between the laser and inner wall in X axis. They are implicitly obtained from the following relations:

$$x_0{}^2 + y_0{}^2 = Dy_0, \tag{5}$$

$$y_0 = y_{\mathrm{m}} - \frac{x_0}{\tan\theta_{\mathrm{w}}}, \tag{6}$$

$$x_0 = (D/2)\sin(\theta_{\mathrm{w}} - \theta'_{\mathrm{w}}), \tag{7}$$

$$\frac{\sin\theta'_{\mathrm{w}}}{\sin\theta'_{\mathrm{f}}} = \frac{n_{\mathrm{f}}}{n_{\mathrm{w}}}. \tag{8}$$

From Eqs. (4) to (8), δ_2 is deduced as:

$$\delta_2 = y_{\mathrm{m}} + \frac{1}{2}D\sin(\theta_{\mathrm{w}} - \theta'_{\mathrm{w}})\cdot\left(\frac{1}{\tan(\theta_{\mathrm{w}} - \theta'_{\mathrm{w}} + \theta'_{\mathrm{f}})} - \frac{1}{\tan\theta_{\mathrm{w}}}\right). \tag{9}$$

Finally, liquid film thickness δ can be obtained from Eqs. (2) and (9) as follows:

$$\begin{aligned}\delta = &\frac{1}{2}y_{\mathrm{m}}\left(\frac{\tan\theta_{\mathrm{w}}}{\tan\theta_f} + 1\right)\\ &+ \frac{1}{4}D\sin(\theta_{\mathrm{w}} - \theta'_{\mathrm{w}})\cdot\left(\frac{1}{\tan(\theta_{\mathrm{w}} - \theta'_{\mathrm{w}} + \theta'_{\mathrm{f}})} - \frac{1}{\tan\theta_{\mathrm{w}}}\right).\end{aligned} \tag{10}$$

The curvature effect on liquid film thickness is not so severe when the liquid film is thin. The difference of δ_1 and δ_2 is less than 4% in the present experiments.

2.3 Measurement uncertainties

The experimental uncertainties are shown in Table 3. The bubble velocity is obtained from the images captured by the high speed camera. The size of total image is 512 $\times$ 64 pixels and the error for measuring the position of bubble nose is less than ± 2 pixels. Therefore, uncertainty of the bubble velocity becomes about ± 4 pixels / 256 pixels, i.e., $\pm 1.56\%$. As for the liquid film thickness, the effects of inner wall curvature, vibration of the micro tube, deviation of measurement position from the tube center and the cover glass angle are investigated. Estimated uncertainties are listed in Table 3. Due to inner wall curvature, liquid film thickness is obtained as the average value of δ_1 and δ_2 as shown in Eq. (1). Measurement uncertainty is obtained from the difference of δ_1 and δ_2. Figures 6 (a) and (b) show the measured absolute positions of the cover glass surface and the inner. Figure 6 (c) shows the relative distance from the cover glass surface to the inner wall, which can be also measured directly by laser focus displacement meter. In Figs. 6 (a) and (b), absolute positions of the cover glass and the inner wall vibrate in the range of nearly ± 10 μm. On the contrary, relative distance from the cover glass surface to the inner wall is almost constant within ± 0.5 μm. Thus, relative distance from the cover glass to the inner wall can be measured with small variation although their absolute positions vibrate in a large range. The deviation of measuring position from the tube center affects the measurement of the liquid film thickness. The liquid film thickness is measured thicker as the deviation becomes larger. The deviation of measuring position is less than 3 μm. If the angle of cover glass is not perpendicular to the center line of the laser beam, refraction of laser beam in positive and negative axes becomes different as

shown in Fig 7. Measurement uncertainties when the angle of cover glass is 1° are listed in Table 3.

2.4 Properties of working fluids

It is known that the liquid film thickness in micro tube is mainly determined by the force balance between viscous and surface tension forces, i.e., capillary number. However, it is reported that inertial force should be considered even in micro tubes when Reynolds number becomes relatively large (Heil, 2001). To clarify the effect of inertial force on the liquid film thickness, three working fluids, water, ethanol and FC-40 were used. Gas is air and all experiments were conducted under the condition of room temperature and 1 atm. Table 2 shows the properties of three liquids at 20°C and 25°C. Figure 8 shows the Reynolds number against capillary number for the present experimental condition. Viscosity and density of the liquid phase are used for Reynolds and capillary numbers. Reynolds number of ethanol is about 6 times larger than that of FC-40, and Reynolds number of water is about 6 times larger than that of ethanol at the same capillary number. The effect of inertial force on the liquid film thickness becomes strong in the case of water.

2.5 Experimental procedure

Figure 9 shows a typical liquid film thickness data for water in 1.3 mm inner diameter tube. The liquid film thicknesses were measured from four different directions as shown in Fig. 10. If the angle of interface becomes larger than 11°, intensity of the reflected light becomes weak and the interface position

cannot be detected. Therefore, it is impossible to measure the whole shape of the bubble nose. In Fig. 9, liquid film thickness decreases initially and then becomes nearly constant or changes gradually. Initial decreasing part is the transition region between the bubble nose and the flat film region. The liquid film thickness after the rapid decrease is defined as the initial liquid film thickness δ_0. Liquid film thickness at the tube top decreases linearly, while the liquid film thickness increases linearly at the tube bottom. Thus, the lineal change after the initial drop is attributed to the gravitational effect. The liquid film flows down due to gravity after liquid film is formed on the tube wall. On the other hand, liquid film thickness at the tube side in horizontal flow direction and in vertical flow do not change and remain nearly constant. Regardless of the measuring positions, initial liquid film thicknesses δ_0 are almost the same for this tube diameter and velocity condition.

3 Results and discussion

3.1 The effect of gravity on the initial liquid film thickness

When the effect of gravity becomes dominant, initial liquid film thickness δ_0 takes different values according to the measuring positions. Figure 11 shows the initial liquid film thicknesses measured at different measuring positions in 1.3 mm and 0.3 mm inner diameter tubes using FC-40. Initial liquid film thicknesses vary according to the measuring positions in $D = 1.3$ mm tube. Initial liquid film thicknesses at the tube side in horizontal flow direction and in vertical flow direction are identical. On the other hand, initial liquid film thicknesses in $D = 0.3$ mm tube are identical regardless of the measuring

positions.

Figure 12 shows the criterion for the gravitational effect on the initial liquid film thickness. In Fig. 12, cross marks correspond to the case when the initial liquid film thickness at the tube bottom is more than 5% larger than that at the tube side, i.e., $1.05\delta_{0\_side} < \delta_{0\_bottom}$, and open symbols are for $\delta_{0\_side} \leq \delta_{0\_bottom} \leq 1.05\delta_{0\_side}$. The difference of the liquid film thicknesses at the tube bottom and the tube side is affected not only by Bond number but also by capillary number. As Bond number and capillary number increase, the difference between δ_{0_bottom} and δ_{0_side} becomes larger. In Fig. 12, dotted lines show the criterion for gravitational effect on the liquid film thickness in each working fluid. Initial liquid film thickness of water at the tube bottom becomes thicker at smaller capillary numbers. Reynolds number of water flow is quite large even at small capillary number. The reason may be attributed to the effect of flow transition from laminar to turbulent.

3.2 The effects of bubble and liquid slug lengths

In the present experiment, liquid is pulled by an actuator motor. Thus, the flow can be considered as a very long bubble behind a very long liquid slug. In reality, bubble length and liquid slug length could be shorter and they may affect the liquid film thickness. The effects of bubble and liquid slug lengths were investigated using water as a working fluid. The liquid film thickness is measured at the tube side in horizontal flow direction. An isolated air bubble and a liquid slug are injected from the open edge of the micro tube. Bubble and liquid slug lengths are measured from the images captured by the high speed camera. Figure 13 shows the schematic diagram of a short bubble and a

liquid slug. Bubble length L_{bubble} and liquid slug length L_{slug} vary within the range of $D < L_{\mathrm{bubble}} < 6D$ and $0 < L_{\mathrm{slug}} < 3D$. Figure 14 shows the measured δ_0 with different L_{bubble} and L_{slug}. In Fig. 14, δ_{0_slug} means the initial liquid film thickness behind liquid slug and $\delta_{0\_\mathrm{bubble}}$ means the initial liquid film thickness in a bubble. In Fig. 14 (a), $\delta_{0\_\mathrm{bubble}}$ of all cases are almost identical with the case of long liquid slug. It seems that L_{slug} has a weak effect on the liquid film thickness. When $Ca < 0.01$, liquid film thickness seems to be independent on the bubble length if bubble length becomes 2 times larger than inner diameter. However, liquid film is thicker for short bubbles, $L_{\mathrm{bubble}} < 2D$. It is considered that the liquid film thickness in a short bubble becomes thicker because the bubble tail also affects δ_0. On the other hand, at high capillary numbers, liquid film thickness becomes thicker even in long bubbles and large deviations are observed in Fig. 14 (b). According to Bretherton's theory (1961), transition region length between the bubble nose and the flat film region is proportional to the capillary number. It is considered that the transition region becomes longer as capillary number increases.

3.3 FC-40/air experiment

Figure 15 (a) shows the liquid film thickness against velocity for FC-40/air experiment. Liquid film thickness measured at the tube side in horizontal flow direction is used. Liquid film thickness increases with bubble velocity and tube diameter. It is known that the liquid film thickness is mainly determined by the force balance between viscous and surface tension forces, which can be represented by capillary number $Ca = \mu U/\sigma$. Viscous force makes liquid film thicker and surface tension makes liquid film thinner. The effect of viscous

force becomes dominant as the bubble velocity increases and the effect of surface tension becomes smaller as tube diameter increases.

Figure 15 (b) shows the dimensionless liquid film thickness δ_0/D against capillary number, using the same data in Fig. 15 (a). The solid line in Fig. 15 (b) is an empirical fitting curve of Taylor's experimental data proposed by Aussillous and Quere (2000).

$$\frac{\delta_0}{D} = \frac{0.67Ca^{\frac{2}{3}}}{1 + 2.5\times1.34Ca^{\frac{2}{3}}}. \tag{11}$$

Equation (11) is called the Taylor's law. The working fluids in Taylor's experiments were highly viscous such as glycerol and sugar-water syrup. Therefore, Reynolds number in Taylor's experiment was small and the inertial force is negligible. At $Ca < 0.025$, dimensionless liquid film thicknesses of five tubes become nearly identical with Taylor's law. Thus, the inertial force can be neglected and the dimensionless liquid film thickness is determined only by capillary number. As capillary number increases, all data become smaller than the Taylor's law. At $0.025 < Ca < 0.10$, liquid film thickness decreases as tube diameter increases. For example, liquid film thickness of 1.3 mm inner diameter tube is lower than that of 0.3 mm inner diameter tube at $Ca \approx 0.05$. Reynolds numbers of 1.3 mm and 0.3 mm inner diameter tubes are $Re = 151$ and 34 at $Ca = 0.05$. As capillary number increases, this trend is inverted. At $Ca > 0.15$, liquid film thickness increases as Reynolds number increases.

3.4 Ethanol/air experiment

As shown in Fig. 8, Reynolds number of ethanol is about 6 times larger than that of FC-40. Therefore, the effect of inertial force becomes stronger

for ethanol than for FC-40. Figure 16 (a) shows the liquid film thickness for ethanol. Again, liquid film thicknesses measured from the tube side are used. Figure 16 (b) shows the dimensionless film thickness against capillary number. At $Ca < 0.02$, the dimensionless liquid film thicknesses in five different tubes become nearly identical with the Taylor's law as in the case of FC-40. However, the deviation from the Taylor's law starts from lower capillary number as Reynolds number increases. At large capillary numbers, all data are larger than the Taylor's law. inertial force is often neglected in micro two-phase flows but it is shown that the inertial force should be considered at relatively large Reynolds number. In Fig. 16 (b), dimensionless liquid film thickness in 1.3 mm inner diameter tube shows different trend at $Ca > 0.12$. For $Ca > 0.12$, liquid film thickness does not increase with capillary number but remains nearly constant. Reynolds number of ethanol in 1.3 mm inner diameter tube becomes 2000 at $Ca \approx 0.12$. Thus, this different trend is considered to be the effect of flow transition from laminar to turbulent.

3.5 Water/air experiment

Figure 17 (a) shows the liquid film thickness against bubble velocity for water. At $Re > 2000$, liquid film thickness does not increase but remains nearly constant with some scattering. In Fig. 17 (a), points of $Re \approx 2000$ in each tube is indicated. Thus, this trend is considered to be the flow transition of the liquid phase from laminar to turbulent. Figure 17 (b) shows the dimensionless film thickness against capillary number for water. The deviation from Taylor's law starts from the lower capillary number $Ca \approx 0.01$, compared with the cases of FC-40 and ethanol. Dimensionless liquid film thicknesses of water show much

larger values than that of ethanol and Taylor's law. In the case of 1.3 mm inner diameter tube, dimensionless liquid film thickness is nearly 2 times larger than the Taylor's law at $Ca \approx 0.03$. It is obvious that inertial force has a strong effect on the liquid film thickness at relatively large Reynolds number.

3.6 The effect of Reynolds number

Figure 18 shows the measured dimensionless liquid film thickness with the numerical simulation results obtained by Kreutzer et al. (2005). Dimensionless liquid film thickness at a particular capillary number is obtained from the fitting curve of the experimental data. Dimensionless liquid film thicknesses are nearly constant against Reynolds number at small capillary number. Therefore, at small capillary numbers, inertial force can be neglected and liquid film thickness is determined only by capillary number. As capillary number increases, the dimensionless liquid film thickness is not constant against Reynolds number. At small Reynolds numbers, the dimensionless liquid film thickness decreases as Reynolds number increases. As Reynolds number increases further, the dimensionless liquid film thickness takes a minimum and then increases. This effect of inertial force on the liquid film thickness is reported in the several numerical simulation studies (Heil, 2001; Kreutzer et al., 2005).

3.7 Scaling analysis

Aussillous and Quere (2000) replaced the curvature of the bubble nose $\kappa = 1/(D/2)$ with $\kappa = 1/\{(D/2)\text{-}\delta_0\}$ in Bretherton's theroritical analysis (1961),

and obtained the following relation:

$$\frac{\delta_0}{D/2} \sim \frac{Ca^{\frac{2}{3}}}{1+Ca^{\frac{2}{3}}}. \tag{12}$$

In Eq. (12), dimensionless liquid film thickness asymptotes to a finite value due to the term $Ca^{2/3}$ in the denominator. Based on Eq. (12), Taylor's experimental data was fitted as Eq. (11). In Fig. 19, if the effect of inertial force is taken into account, the momentum balance and the curvature matching between the bubble nose and the transition region should be expressed as follows:

$$\frac{\mu U}{\delta_0^2} \sim \frac{1}{\lambda}\left\{\frac{\sigma}{(D/2)-\delta_0}\right\} - \frac{1}{\lambda}\rho U^2, \tag{13}$$

$$\frac{\delta_0}{\lambda^2} \sim \frac{1}{(D/2)-\delta_0}. \tag{14}$$

We can deduce the relation of δ_0/D from Eqs. (13) and (14) as:

$$\frac{\delta_0}{D} \sim \frac{Ca^{\frac{2}{3}}}{Ca^{\frac{2}{3}}+(1-We')^{\frac{2}{3}}}, \tag{15}$$

where Weber number is defined as $We' = \rho U^2((D/2)\text{-}\delta_0)/\sigma$. Equation (15) is always larger than Eq. (12) because the sign in front of Weber number is negative. Therefore, Eq. (15) can express the increase of the liquid film thickness with Weber number. On the other hand, Heil (2001) reported that at finite Reynolds number, inertial force makes the bubble nose slender and increases the bubble nose curvature. It is reported in Edvinsson and Irandoust (1996) and Kreutzer et al. (2005) that the curvature of bubble nose increases with Reynolds number and capillary number. This implies that curvature term $\kappa = 1/\{(D/2)\text{-}\delta_0\}$ in momentum equation should be larger with Reynolds number and capillary number. We assume that this effect of curvature change can be expressed by adding a function of Reynolds number and capillary

number to $\kappa = 1/\{(D/2)\text{-}\delta_0\}$ term as:

$$\kappa = \frac{1 + f(Re, Ca)}{(D/2) - \delta_0}. \tag{16}$$

Substituting Eq. (16) in Eqs. (13) and (14), we can obtain the following relations:

$$\begin{aligned}
\frac{\mu U}{\delta_0^2} &\sim \frac{1}{\lambda}\left\{\frac{\sigma\,(1 + f(Re, Ca))}{(D/2) - \delta_0}\right\} - \frac{1}{\lambda}\rho U^2, \\
\frac{\delta_0}{\lambda^2} &\sim \frac{(1 + f(Re, Ca))}{(D/2) - \delta_0}, \\
\frac{\delta_0}{(D/2)} &\sim \frac{Ca^{\frac{2}{3}}}{Ca^{\frac{2}{3}} + (1 + f(Re, Ca))(1 - \frac{We'}{1+f(Re,Ca)})^{\frac{2}{3}}}.
\end{aligned} \tag{17}$$

If we assume that the terms of Re, Ca and We are small, we may simplify Eq. (17) using Taylor expansion as:

$$\frac{\delta_0}{(D/2)} \sim \frac{Ca^{\frac{2}{3}}}{Ca^{\frac{2}{3}} + 1 + f(Re, Ca) - g(We')}. \tag{18}$$

In the denominator of Eq. (18), $f(Re,Ca)$ term corresponds to the curvature change of bubble nose and contributes to reduce the liquid film thickness. On the contrary, when the inertial effect increases, $g(We')$ term contributes to increase the liquid film thickness due to the inertial term in the momentum equation. Weber number in Eq. (15) includes the liquid film thickness δ_0 in its definition. Therefore, in order to simplify the correlation, Weber number is redefined as $We = \rho U^2 D/\sigma$. Experimental data is finally correlated in the form as:

$$\frac{\delta_0}{D} = \begin{cases} \dfrac{0.670 Ca^{\frac{2}{3}}}{1+3.13 Ca^{\frac{2}{3}} + 0.504 Ca^{0.672} Re^{0.589} - 0.352 We^{0.629}} & (Re < 2000) \\ \dfrac{106.0\left(\frac{\mu^2}{\rho\sigma}\cdot\frac{1}{D}\right)^{\frac{2}{3}}}{1+497.0\left(\frac{\mu^2}{\rho\sigma}\cdot\frac{1}{D}\right)^{\frac{2}{3}} + 7330\left(\frac{\mu^2}{\rho\sigma}\cdot\frac{1}{D}\right)^{0.672} - 5000\left(\frac{\mu^2}{\rho\sigma}\cdot\frac{1}{D}\right)^{0.629}} & (Re > 2000), \end{cases} \tag{19}$$

where $Ca = \mu U/\sigma$ and $Re = \rho UD/\mu$ and $We = \rho U^2 D/\sigma$. As capillary number approaches zero, the first equation of Eq. (19) for $Re < 2000$ should follow Bretherton's theory, so the coefficient in the numerator is taken as 0.670. The other coefficients are obtained by least linear square method from the present experimental data. If Reynolds number becomes larger than 2000, liquid film thickness remains constant due to the flow transition from laminar to turbulent. Therefore, liquid film thickness is fixed to the value at $Re = 2000$. The second equation of Eq. (19) for $Re > 2000$ can be obtained from the first equation by substituting $Re = 2000$. Capillary number and Weber number should be also replaced with the values when Reynolds number is 2000. The first equation of Eq. (19) are replaced as follows:

$$Ca = Re \times \left(\frac{\mu^2}{\rho\sigma} \cdot \frac{1}{D}\right) = 2000 \times \left(\frac{\mu^2}{\rho\sigma} \cdot \frac{1}{D}\right) \qquad (Re = 2000), \tag{20}$$

$$We = Re \cdot Ca = 2000^2 \times \left(\frac{\mu^2}{\rho\sigma} \cdot \frac{1}{D}\right) \qquad (Re = 2000). \tag{21}$$

In Eqs. (21) and (22), $(\mu^2/\rho\sigma D)$ is a constant value if tube diameter and fluid properties are fixed. Figures 20 and 21 show the comparison between the experimental data and the prediction of Eq. (19). As shown in Fig. 21, the present correlation can predict δ_0 within the range of $\pm 15\%$ accuracy.

4 Concluding remarks

The initial liquid film thickness in a micro tube is measured directly by laser focus displacement meter. Liquid film thickness changes according to the measuring positions due to gravity. However, the initial liquid film thickness δ_0 is independent of the measuring positions when Bond number and capillary number are small. Liquid slug length has only a weak effect on liquid film

thickness. However, liquid film thickness becomes thicker for short bubbles, $L_{\mathrm{bubble}} < 2D$. At small capillary number, the initial liquid film thickness is determined only by capillary number and inertial effect is negligible. As capillary number increases, the effect of inertial force can not be neglected. At relatively large capillary number, liquid film thickness takes a minimum value against Reynolds number. If Reynolds number becomes larger than roughly 2000, liquid film thickness becomes nearly constant and shows some scattering. Empirical correlation for the dimensionless liquid film thickness based on capillary number, Reynolds number and Weber number is proposed. The proposed correlation can predict the initial liquid film thickness within $\pm 15\%$ accuracy.

Acknowledgements

We would like to thank Prof. Kasagi, Prof. Suzuki and Dr. Hasegawa for the fruitful discussions and suggestions. This work is supported through Grant in Aid for Scientific Research (No. 20560179) by MEXT, Japan.

References

Aussillous, P., Quere, D., 2000. Quick deposition of a fluid on the wall of a tube, *Phys. of Fluids*, 12(10), 2367-2371.

Bretherton, F. P., 1961. The motion of long bubbles in tubes, *J. Fluid Mech.*, 10(2), 166-188.

Edvinsson, R. K., Irandoust, S., 1996. Finite-element analysis of taylor flow,

AIChE J., 42(7), 1815-1823.

Hazuku, T., Fukamachi, N., Takamasa, T., Hibiki, T., Ishii, M., 2005. Measurement of liquid film in microchannels using a laser focus displacement meter, *Experiments in Fluids*, 38(6), 780-788.

Heil, M., 2001. Finite Reynolds number effects in the Bretherton problem, *Phys. of Fluids*, 13(9), 2517-2521.

Kenning, D. B. R., Wen, D. S., Das, K. S., Wilson, S. K., 2006. Confined growth of a vapour bubble in a capillary tube at initially uniform superheat: Experiments and modeling, *Int. J. Heat Mass Transfer*, 49(23-24), 4653-4671.

Kreutzer, M. T., Kapteijn, F., Moulijn, J. A., Kleijn, C. R., Heiszwolf, J. J., 2005. Inertial and interfacial effects on pressure drop of Taylor flow in capillaries, *AIChE J.*, 51(9), 2428-2440.

Moriyama, K., Inoue, A., 1996. Thickness of the liquid film formed by a growing bubble in a narrow gap between two horizontal plates, *Trans. of the ASME*, 118, 132-139.

Takamasa, T., Kobayashi, K., 2000. Measuring interfacial waves on film flowing down tube inner wall using laser focus displacement meter, *J. Multiphase Flow*, 26(9), 1493-1507.

Taylor, G. I., 1961. Deposition of a viscous fluid on the wall of a tube, *J. Fluid Mech.*, 10(2), 161-165.

Thome, J. R., Dupont, V., Jacobi, A. M., 2004. Heat transfer model for evaporation in microchannels. Part I: presentation of the model, *Int. J. Heat Mass Transfer*, 47(14-16), 3375-3385.

Utaka, Y., Okuda, S., Tasaki, Y., 2007. Structure of micro-layer and characteristics of boiling heat transfer in narrow gap mini-channel system, *Trans. of the JSME, Series B*, 73(733), 1929-1935.

Appendix

Measured data and the flow conditions are listed in Tables A-1 to A-3. Initial liquid film thicknesses are measured from the tube side. Temperatures for each of test runs are is also listed.

Table A-1

Bubble velocity U against initial liquid film thickness δ_0 for FC-40

D = 1.305 mm		D = 0.995 mm		D = 0.715 mm		D = 0.487 mm		D = 0.305 mm	
T = 21.8°C		T = 21.7°C		T = 21.2°C		T = 21.8°C		T = 21.5°C	
U (m/s)	δ_0 (μm)	U (m/s)	δ_0 (μm)	U (m/s)	δ_0 (μm)	U (m/s)	δ_0 (μm)	U (m/s)	δ_0 (μm)
0.007	11.7	0.007	9.9	0.031	16.8	0.030	10.0	0.049	8.8
0.009	12.4	0.023	18.8	0.068	25.4	0.042	12.9	0.081	12.0
0.013	16.8	0.036	23.8	0.110	31.6	0.052	14.2	0.140	15.7
0.027	24.0	0.048	28.5	0.158	37.5	0.070	18.2	0.162	16.7
0.034	29.2	0.062	33.5	0.142	37.1	0.083	18.9	0.196	18.2
0.042	33.0	0.077	36.9	0.176	41.6	0.100	21.5	0.212	18.6
0.057	38.0	0.090	39.5	0.194	43.3	0.110	22.3	0.269	20.5
0.073	43.1	0.105	41.7	0.234	46.1	0.120	22.9	0.324	21.6
0.089	49.4	0.120	45.5	0.250	47.6	0.159	26.1	0.403	23.8
0.105	53.6	0.137	48.0	0.276	48.6	0.183	27.3	0.462	24.7
0.122	55.2	0.149	49.9	0.308	50.7	0.207	29.1	0.499	25.6
0.139	59.4	0.164	51.4	0.355	54.5	0.273	31.9	0.523	25.2
0.155	62.8	0.180	53.1	0.397	54.8	0.265	31.9	0.642	26.0
0.180	66.6	0.203	55.9	0.451	58.0	0.354	34.7	0.729	27.3
0.200	69.7	0.231	58.7	0.486	59.5	0.389	35.8	0.920	29.2
0.217	70.4	0.259	60.8	0.515	60.0	0.411	36.4	0.928	28.8
0.240	73.4	0.297	64.5	0.566	63.0	0.444	36.8	0.976	29.8
0.268	77.5	0.329	66.5	0.596	63.3	0.437	37.6	1.123	30.7
0.291	79.7	0.367	70.2	0.685	66.6	0.503	39.5	1.279	31.7
0.308	82.1	0.403	72.0	0.689	66.7	0.541	39.3	1.475	32.9
0.342	86.1	0.428	73.5	0.705	67.3	0.554	40.0	1.577	33.3
0.370	88.1	0.479	77.8	0.770	68.5	0.601	41.0	2.115	35.3
0.386	89.0	0.515	78.5	0.830	70.7	0.585	40.9		
0.414	92.7	0.552	81.8	0.837	70.4	0.593	40.5		
0.438	95.6	0.595	84.3	0.863	72.3	0.657	41.9		
0.495	103.7	0.633	86.9	0.951	74.0	0.871	45.3		
0.501	101.8	0.721	90.9	1.013	74.4	0.927	45.9		
0.565	108.9	0.741	91.9	1.093	78.3	0.961	46.6		
0.590	109.8	0.773	93.7	2.221	88.9	0.965	46.6		
0.615	115.0	0.842	96.1	3.131	94.1	1.244	50.0		
0.635	121.1	0.909	103.3	4.681	94.7	1.527	52.2		
0.646	112.9	0.965	106.6			2.102	55.5		
0.686	118.5	1.025	108.1			2.362	57.1		
0.689	118.1	1.084	108.6						
0.721	124.1	1.091	108.0						
0.806	128.7	1.159	107.0						
		1.227	112.2						

Table A-2

Bubble velocity U against initial liquid film thickness δ_0 for ethanol

D = 1.305 mm		D = 0.995 mm		D = 0.715 mm		D = 0.487 mm		D = 0.305 mm	
T = 21.5°C		T = 20.3°C		T = 20.8°C		T = 21.4°C		T = 20.4°C	
U (m/s)	δ_0 (μm)	U (m/s)	δ_0 (μm)	U (m/s)	δ_0 (μm)	U (m/s)	δ_0 (μm)	U (m/s)	δ_0 (μm)
0.012	6.3	0.056	13.1	0.021	6.8	0.047	6.9	0.082	3.7
0.025	10.5	0.118	22.1	0.042	8.3	0.092	9.1	0.149	7.0
0.052	17.2	0.119	16.7	0.060	11.8	0.093	9.4	0.230	9.8
0.066	20.5	0.242	33.2	0.084	12.9	0.096	9.4	0.407	12.3
0.133	25.8	0.247	34.7	0.109	13.3	0.203	16.1	0.468	13.8
0.138	40.8	0.322	38.1	0.131	16.8	0.199	14.3	0.477	14.0
0.145	32.5	0.337	38.5	0.155	18.6	0.222	15.1	0.527	14.7
0.178	39.9	0.445	40.1	0.216	21.6	0.312	17.4	0.600	15.2
0.208	37.7	0.450	40.4	0.226	24.2	0.357	18.9	0.645	16.1
0.243	43.0	0.516	49.1	0.297	24.6	0.417	19.2	0.686	16.6
0.285	45.1	0.517	46.8	0.312	25.2	0.574	22.1	0.746	17.0
0.286	47.8	0.607	50.3	0.407	28.0	0.665	23.8	0.800	17.2
0.333	53.9	0.617	47.5	0.463	30.6	0.707	24.4	0.902	18.3
0.366	46.0	0.740	59.0	0.472	32.2	0.766	25.7	0.998	19.0
0.373	51.1	0.761	55.9	0.490	32.2	0.772	26.3	1.174	19.9
0.443	59.7	0.843	63.2	0.602	35.1	0.820	26.1	1.269	21.4
0.453	51.1	0.844	62.7	0.646	36.4	0.915	27.8	1.439	21.9
0.455	65.3	0.996	71.7	0.716	39.3	0.946	30.5	1.544	22.4
0.528	62.1	1.015	69.9	0.728	38.4	1.064	28.9	1.551	22.8
0.531	59.6	1.197	78.2	0.851	43.6	1.049	29.7	1.821	24.0
0.531	67.8	1.216	77.5	0.886	43.1	1.143	32.3	1.886	24.2
0.620	75.2	1.388	89.3	1.029	48.9	1.244	34.0	2.004	24.8
0.708	74.9	1.423	81.5	1.058	51.0	1.272	32.6	2.028	25.5
0.707	83.7	1.594	90.0	1.072	49.5	1.334	37.0	2.071	25.5
0.788	80.4	1.585	91.5	1.087	47.1	1.269	33.1	2.251	26.2
0.804	84.5	1.717	97.2	1.308	58.4	1.392	35.1	2.399	27.1
0.818	90.8	1.876	98.8	1.405	54.8	1.479	37.1	2.440	26.9
1.011	92.6	1.919	102.2	1.424	57.4	1.412	35.3	2.617	27.5
1.026	99.2	2.021	103.3	1.611	61.8	1.623	39.3	2.872	27.9
1.175	94.5	2.039	104.7	1.792	64.7	1.744	38.2	2.889	28.7
1.235	101.6	2.110	111.4	1.824	65.8	1.671	39.1	3.160	29.0
1.230	106.7	2.149	105.2	1.973	68.8	1.841	41.9		
1.436	114.0	2.249	111.0	1.981	69.5	1.839	41.3		
1.473	120.8	2.390	121.8	2.360	72.6	2.128	44.1		
1.606	121.3	2.390	106.7	2.470	77.1	2.136	40.5		
1.714	133.2	2.509	121.0	2.681	76.2	2.036	42.3		
1.949	123.3	2.673	119.5	2.887	76.9	2.194	43.4		
1.957	126.4	2.809	116.1	3.201	80.6	2.369	43.7		
1.943	139.6	2.946	122.2	3.405	83.7	2.339	45.2		
2.228	140.3	3.040	120.8	3.475	87.5	2.565	47.2		
2.655	134.9	3.096	123.0	4.228	89.7	3.001	50.5		
2.941	130.4	3.163	123.0	4.391	90.3	3.272	53.2		
		3.377	124.0	4.858	97.9	4.207	58.3		
		3.406	123.8	5.026	85.5	4.267	56.8		
		3.467	119.4	5.153	91.1	4.791	61.6		
		3.571	124.2	6.506	92.6	6.078	63.1		
		4.085	135.2			6.877	59.2		
		4.721	146.9			6.965	57.7		
		4.783	130.2						

Table A-3

Bubble velocity U against initial liquid film thickness δ_0 for water

D = 1.305 mm		D = 0.995 mm		D = 0.715 mm		D = 0.487 mm		D = 0.305 mm	
T = 20.3°C		T = 20.5°C		T = 20.5°C		T = 20.7°C		T = 20.2°C	
U (m/s)	δ_0 (μm)	U (m/s)	δ_0 (μm)	U (m/s)	δ_0 (μm)	U (m/s)	δ_0 (μm)	U (m/s)	δ_0 (μm)
0.062	8.3	0.109	9.3	0.083	6.2	0.158	6.1	0.097	2.1
0.111	11.4	0.110	8.9	0.112	6.2	0.178	5.9	0.133	2.9
0.201	17.2	0.114	11.5	0.210	10.2	0.191	4.8	0.240	4.3
0.267	17.9	0.219	9.7	0.218	10.2	0.304	7.6	0.291	4.6
0.354	27.4	0.243	12.0	0.300	12.8	0.357	7.8	0.330	5.9
0.361	23.4	0.332	17.9	0.434	14.6	0.378	9.2	0.418	6.6
0.473	30.3	0.350	16.2	0.440	15.1	0.450	10.1	0.553	8.2
0.545	33.3	0.431	22.0	0.680	19.8	0.520	11.9	0.727	9.3
0.653	39.0	0.462	22.7	0.953	26.3	0.761	14.0	0.779	9.1
0.697	44.4	0.574	25.9	1.037	27.4	0.775	13.8	0.966	10.2
0.807	48.0	0.622	26.8	1.080	28.6	1.029	17.8	1.041	12.4
0.870	53.1	0.694	31.4	1.119	29.0	1.054	18.5	1.253	12.8
0.968	55.3	0.761	30.3	1.130	30.0	1.212	21.0	1.454	14.5
1.046	61.9	0.859	35.0	1.242	32.0	1.379	22.8	1.659	14.5
1.060	62.0	0.873	37.4	1.333	35.7	1.646	26.7	1.706	15.5
1.124	73.2	0.988	42.3	1.402	36.8	1.694	26.9	1.782	15.4
1.154	69.9	1.048	41.4	1.560	41.1	1.764	26.9	1.857	15.9
1.167	68.7	1.084	48.3	1.704	44.2	1.999	32.5	1.964	16.5
1.327	75.0	1.140	43.2	1.815	45.1	2.044	31.8	2.029	16.4
1.328	81.0	1.182	45.9	1.888	48.2	2.245	36.3	2.117	16.9
1.348	84.0	1.317	51.1	1.951	50.3	2.432	36.3	2.381	17.9
1.476	85.6	1.347	52.6	2.134	53.1	2.545	37.5	2.686	20.0
1.519	90.8	1.381	54.7	2.156	53.9	2.757	37.9	2.745	19.6
1.546	93.6	1.408	59.0	2.212	55.9	2.879	39.6	2.810	20.3
1.724	102.4	1.444	55.7	2.445	58.7	2.899	42.2	2.900	20.7
1.791	94.0	1.511	55.2	2.731	61.2	3.088	41.4	3.010	20.7
1.850	102.3	1.606	62.7	3.086	70.1	3.598	45.4	3.335	21.9
1.883	108.5	1.682	58.6	3.250	71.0	3.641	46.2	3.482	23.6
2.011	113.1	1.725	64.2	3.724	74.7	3.903	43.8	3.740	23.9
2.416	95.4	1.761	62.6	4.156	76.0	3.905	45.1	3.808	22.2
2.427	108.3	1.896	71.3	4.378	76.4	4.481	47.2	3.938	23.3
2.595	108.2	1.899	69.8	5.057	80.8	4.513	44.4	4.038	22.8
2.907	103.6	1.977	77.5	5.879	75.8	4.851	47.9	4.122	23.2
		2.079	75.2			5.006	46.9	4.240	23.9
		2.082	72.3			5.205	43.4	4.304	25.1
		2.242	77.7			5.223	46.4	4.554	24.6
		2.404	70.6			5.790	48.5	4.617	25.8
		2.597	70.6			6.040	46.7	4.735	27.2
		2.823	71.5			6.276	48.2	4.809	25.6
		2.871	68.2			6.565	51.1	5.075	28.8
		2.910	64.6					5.108	27.5
		2.954	66.1					5.214	27.6
		3.084	66.5					5.622	28.1
								5.751	28.6
								5.873	29.8
								6.058	28.9
								6.247	30.3

Table 1

Dimensions of the test tubes

I.D. (mm)	O.D. (mm)	Length (mm)
1.305	1.6	250
0.995	1.6	250
0.715	1.0	250
0.487	0.8	250
0.305	0.5	250

Table 2

Properties of the working fluids at 20°C and 25°C

	Temperature	Water	Ethanol	FC-40
ρ (kg/m^3)	20°C	998	789	1860
	25°C	997	785	1849
μ (μ Pa $\cdot$ s)	20°C	1001	1196	3674
	25°C	888	1088	3207
σ (mN/m)	20°C	72.7	22.8	16.3
	25°C	72.0	22.3	15.9
n		1.33	1.36	1.29

Table 3

Experimental uncertainties of the measured values

Quantity		Uncertainty
U_{bubble}	position of bubble nose	±1.56 %
δ_0	inner wall curvature	±1.81% (FC-40, δ_0 = 35.3 μm)
		±1.14% (Ethanol, δ_0 = 92.6 μm)
		±1.24% (Water, δ_0 = 76.4 μm)
δ_0	vibration of micro tube	±0.5 μm
δ_0	deviation from the center	+1.49% (δ_0 = 2 μm)
δ_0	angle of cover glass (1° in X)	+7.47% (FC-40, δ_0 = 5 μm)
δ_0	angle of cover glass (1° in X)	+2.88% (FC-40, δ_0 = 30 μm)
δ_0	angle of cover glass (1° in Z)	+5.76% (FC-40, δ_0 = 5 μm)
δ_0	angle of cover glass (1° in Z)	+1.12% (FC-40, δ_0 = 30 μm)

Fig. 1. Schematic diagram of the experimental setup.

Fig. 2. Cross section of the 0.487 mm inner diameter tube.

Fig. 3. Principle of the laser focus displacement meter.

Fig. 4. Correction for the outer wall curvature.

Fig. 5. Correction for the inner wall curvature.

Fig. 6. Vibration of micro tube during the movement of actuator motor: (a) measured interface position of the cover glass surface (b) measured interface position of the inner wall (c) relative distance between the cover glass surface and the inner wall.

Fig. 7. Schematic diagram for the refraction of laser beam according to the angle of cover glass: (a) X-Y cross section (b) Y-Z cross section.

Fig. 8. Reynolds number against capillary number for the present experiment.

Fig. 9. Measured liquid film thickness against time.

Fig. 10. Schematic diagram for the measuring positions: (a) horizontal flow direction (b) vertical flow direction.

Fig. 11. Initial liquid film thickness δ_0 measured at different positions in FC-40/air experiment: (a) 1.3 mm inner diameter tube (b) 0.3 mm inner diameter tube.

Fig. 12. The gravitational effect on the initial liquid film thickness.

Fig. 13. Schematic diagram of the short bubble and liquid slug.

Fig. 14. The effects of bubble and liquid slug lengths on the liquid film thickness: (a) dimensionless liquid film thickness (δ_{0_slug}/D) behind a liquid slug against capillary number ($Ca = \mu U/\sigma$) (b) dimensionless liquid film thickness (δ_{0_bubble}/D) in a bubble against capillary number ($Ca = \mu U/\sigma$).

Fig. 15. Liquid film thickness of FC-40: (a) liquid film thickness against bubble velocity (b) dimensionless liquid film thickness (δ_0/D) against capillary number ($Ca = \mu U/\sigma$).

Fig. 16. Liquid film thickness of ethanol: (a) liquid film thickness against bubble velocit y (b) dimensionless liquid film thickness (δ_0/D) against capillary number ($Ca = \mu U/\sigma$).

Fig. 17. Liquid film thickness of water: (a) liquid film thickness against bubble velocity (b) dimensionless liquid film thickness (δ_0/D) against capillary number ($Ca = \mu U/\sigma$).

Fig. 18. Dimensionless liquid film thickness (δ_0/D) against Reynolds number ($Re = \rho U D/\mu$).

Fig. 19. Schematic diagram for the scaling analysis on the liquid film thickness.

Fig. 20. Predicted liquid film thickness (δ_0/D) against capillary number ($Ca = \mu U/\sigma$).

Fig. 21. Comparison between prediction and experimental results.

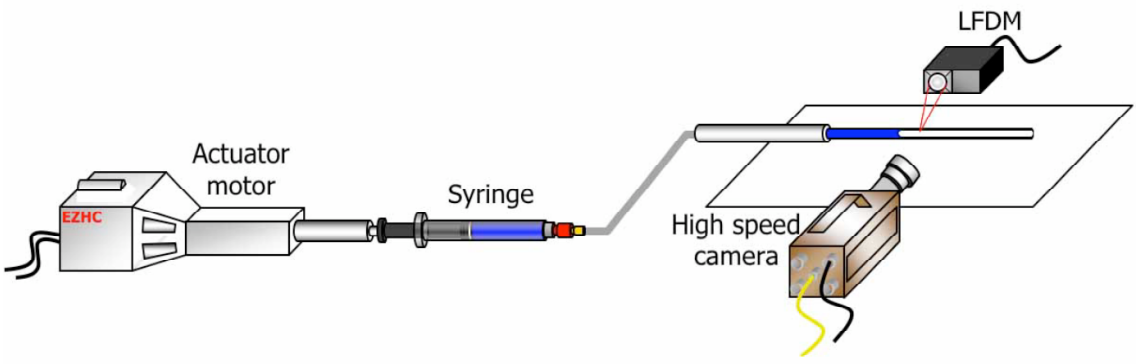

Fig. 1

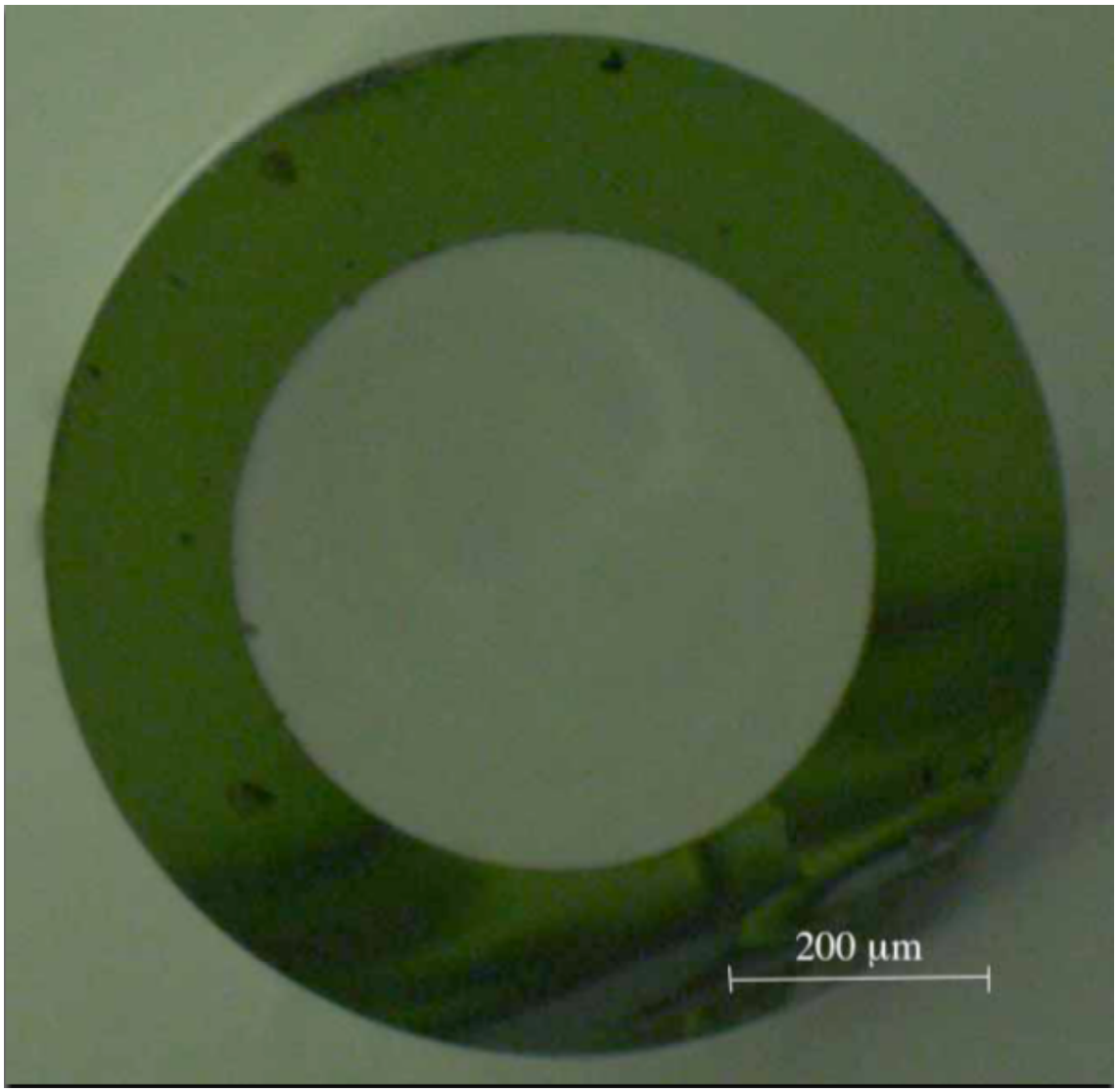

Fig. 2

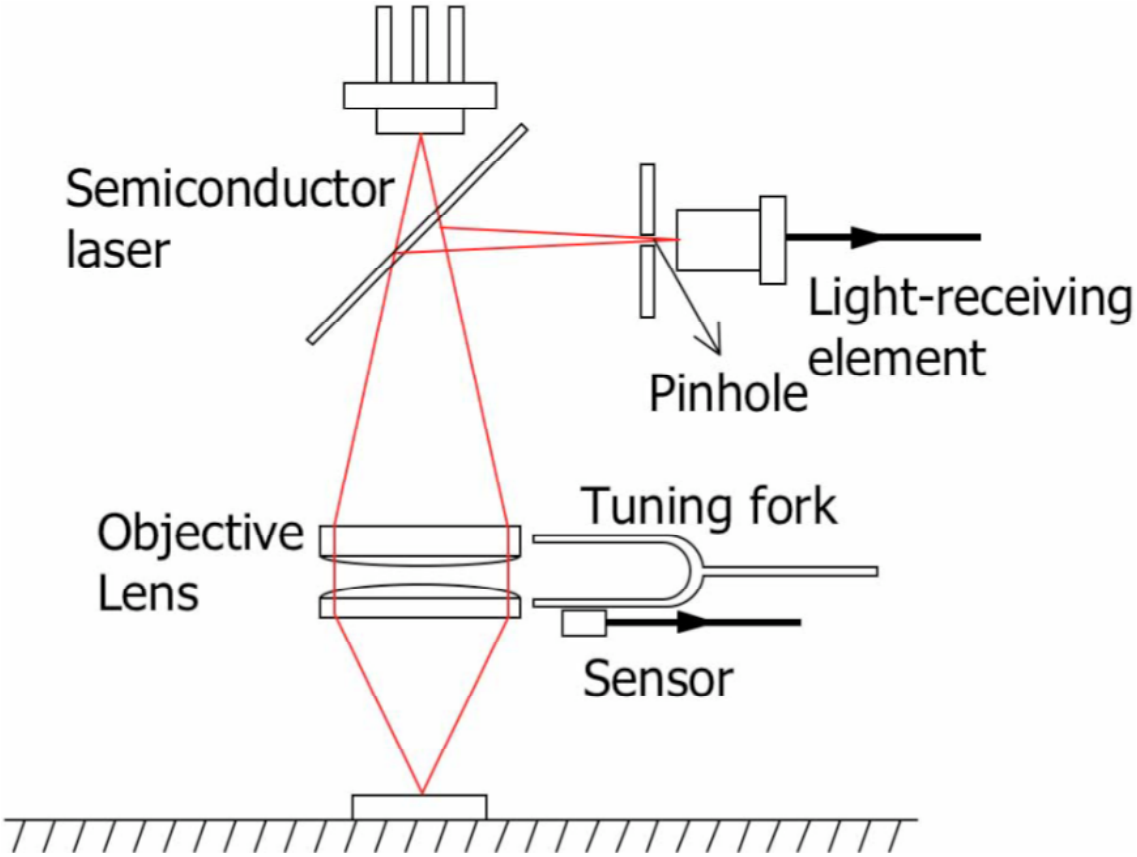
Semiconductor
laser
Light-receiving
element
Pinhole
Tuning fork
Objective
Lens
Sensor

Fig. 3

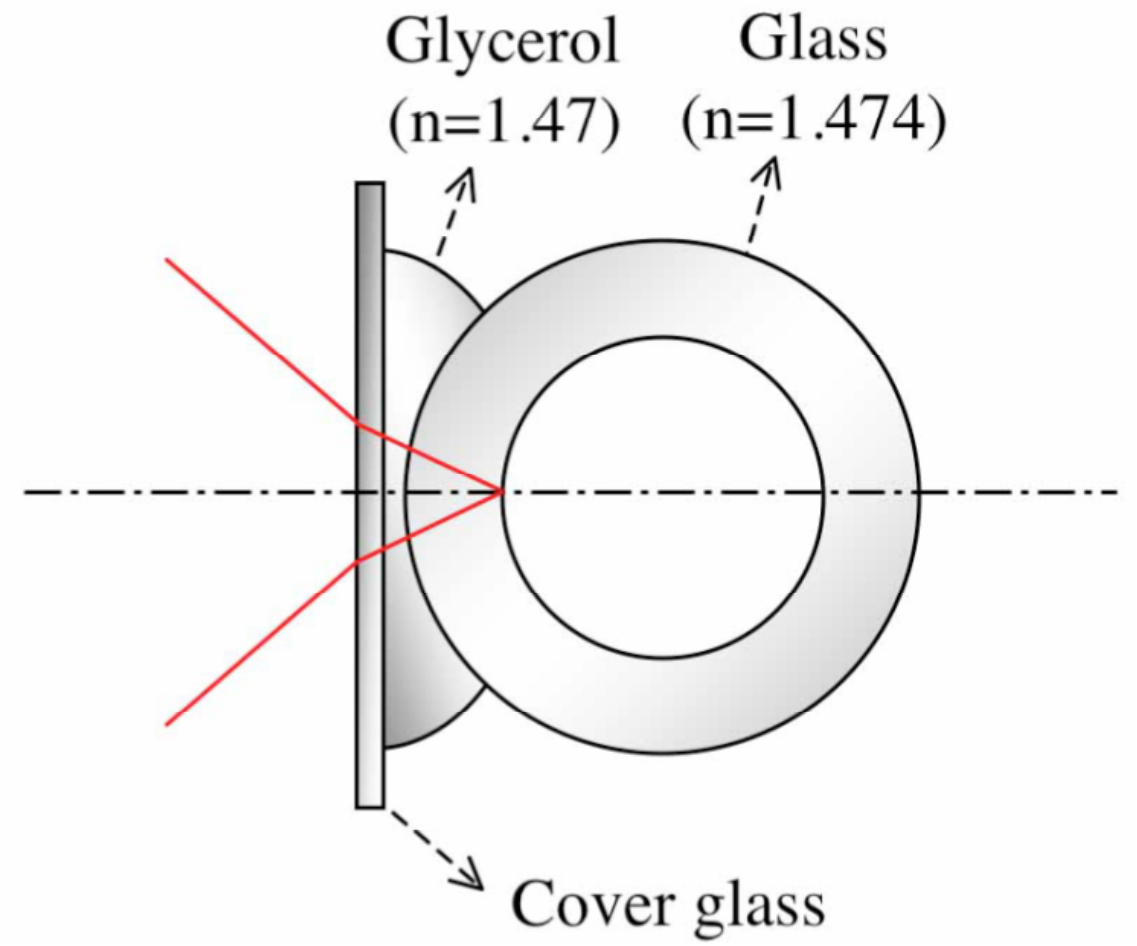
Glycerol
(n=1.47)
Glass
(n=1.474)
Cover glass

Fig. 4

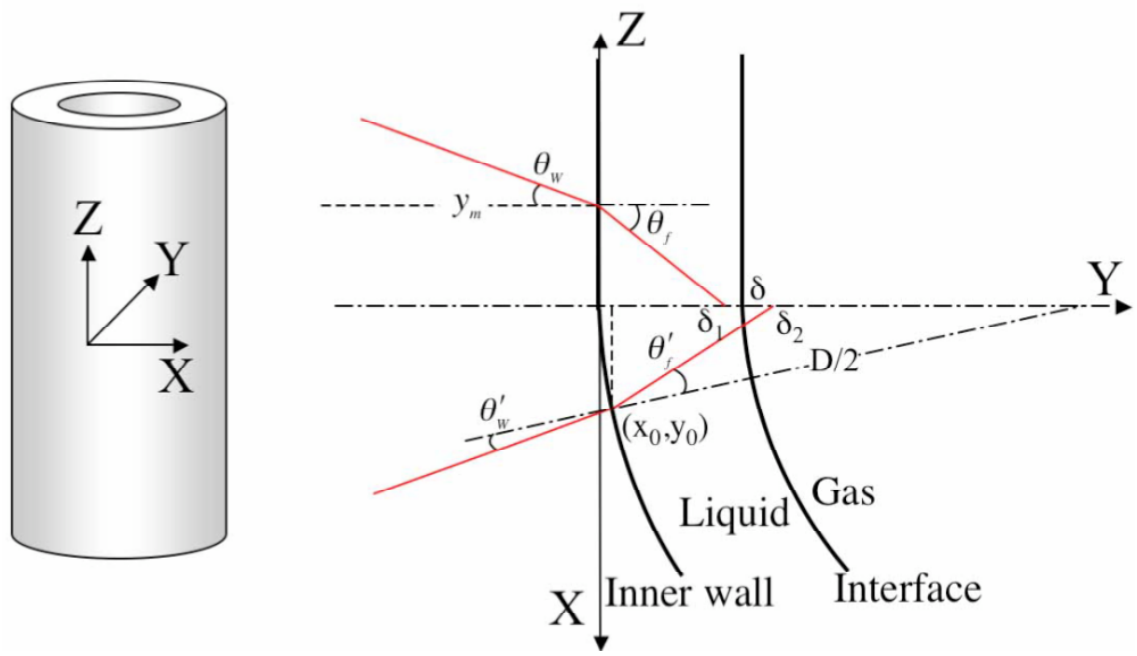
Z
Y
X
Z
θ_w
y_m
θ_f
δ
Y
δ_1
δ_2
θ'_f
D/2
θ'_w
(x_0,y_0)
Liquid
Gas
X
Inner wall
Interface

Fig. 5

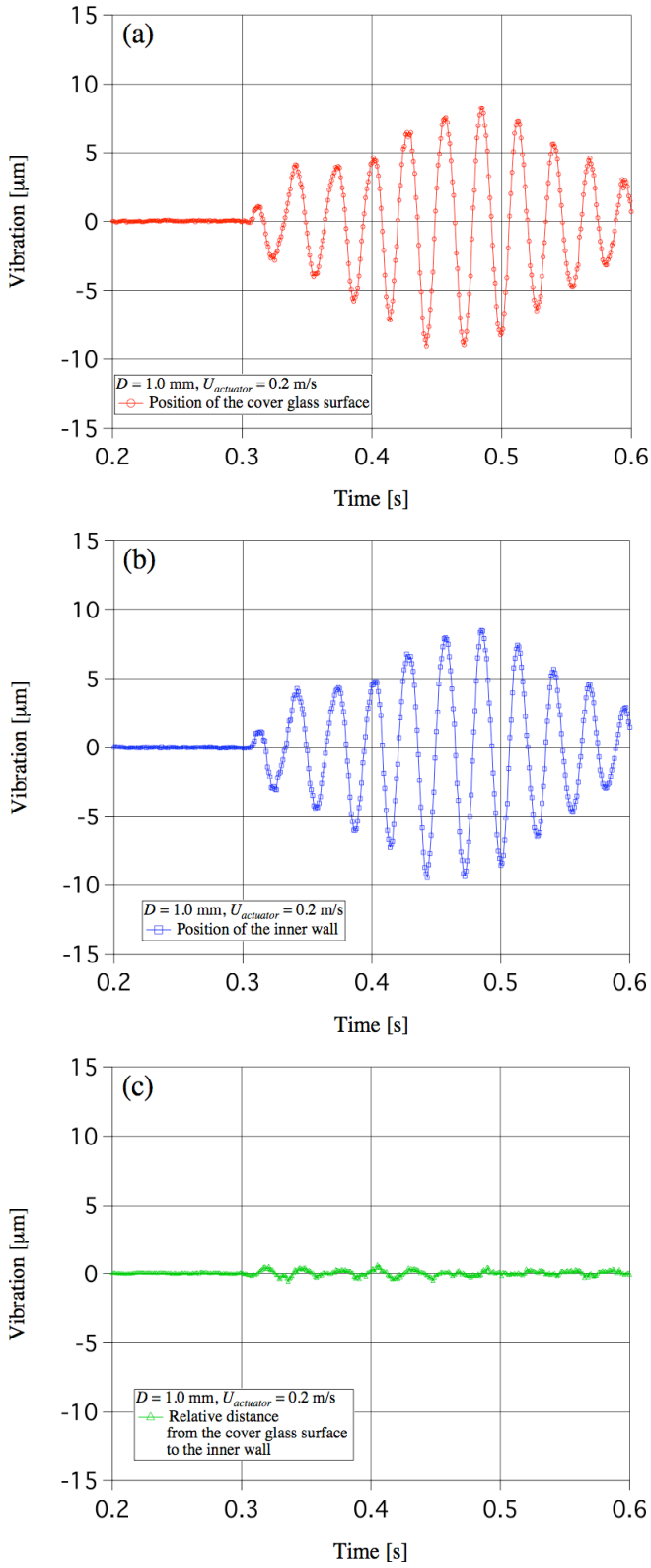
(a)
Vibration [μm]
15
10
5
0
-5
-10
-15
0.2
0.3
0.4
0.5
0.6
Time [s]
D = 1.0 mm, U_actuator = 0.2 m/s
Position of the cover glass surface
(b)
Vibration [μm]
Time [s]
D = 1.0 mm, U_actuator = 0.2 m/s
Position of the inner wall
(c)
Vibration [μm]
Time [s]
D = 1.0 mm, U_actuator = 0.2 m/s
Relative distance
from the cover glass surface
to the inner wall

Fig. 6

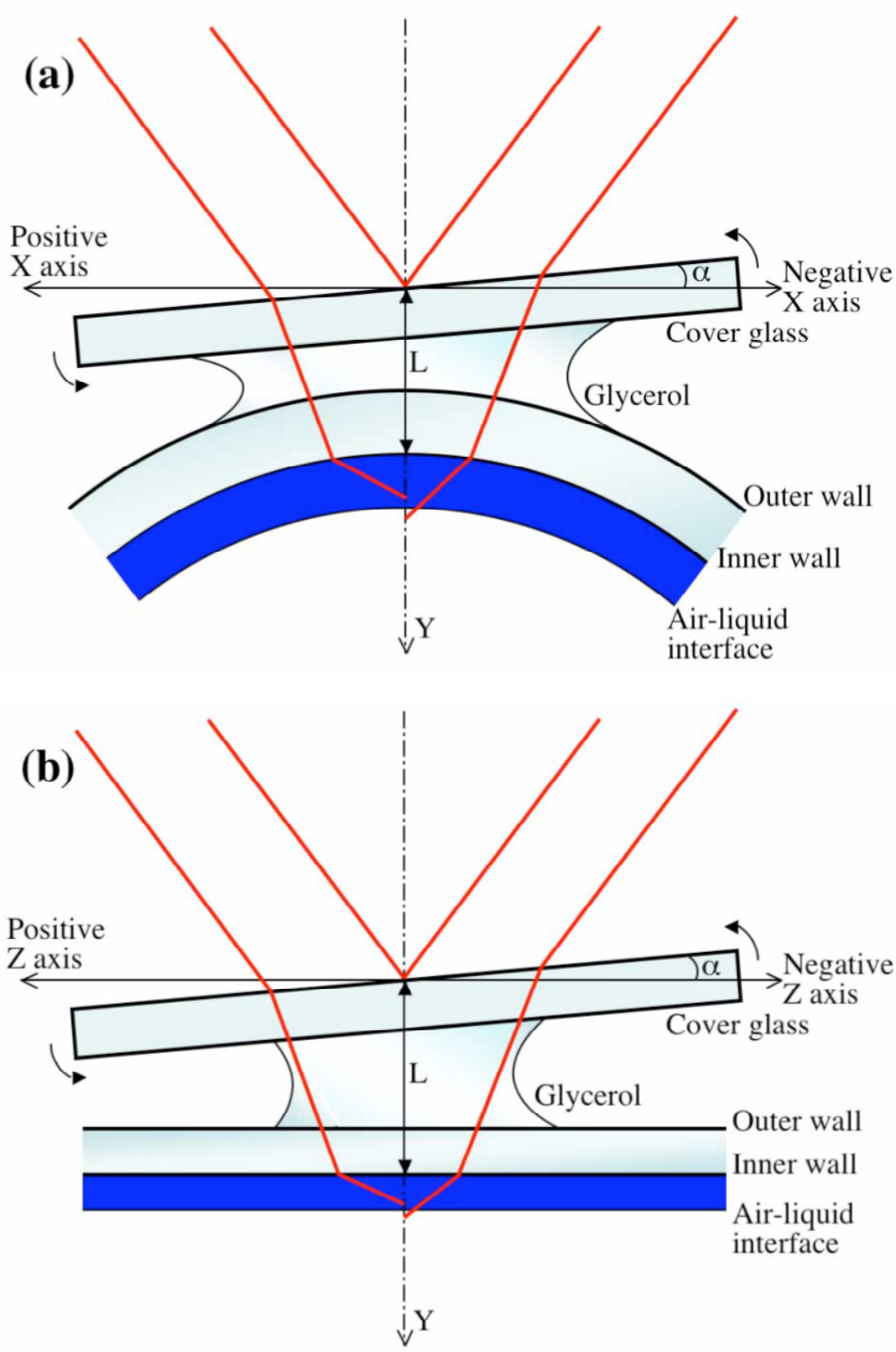
(a)
Positive
X axis
Negative
X axis
α
Cover glass
L
Glycerol
Outer wall
Inner wall
Air-liquid
interface
Y
(b)
Positive
Z axis
Negative
Z axis
α
Cover glass
L
Glycerol
Outer wall
Inner wall
Air-liquid
interface
Y

Fig. 7

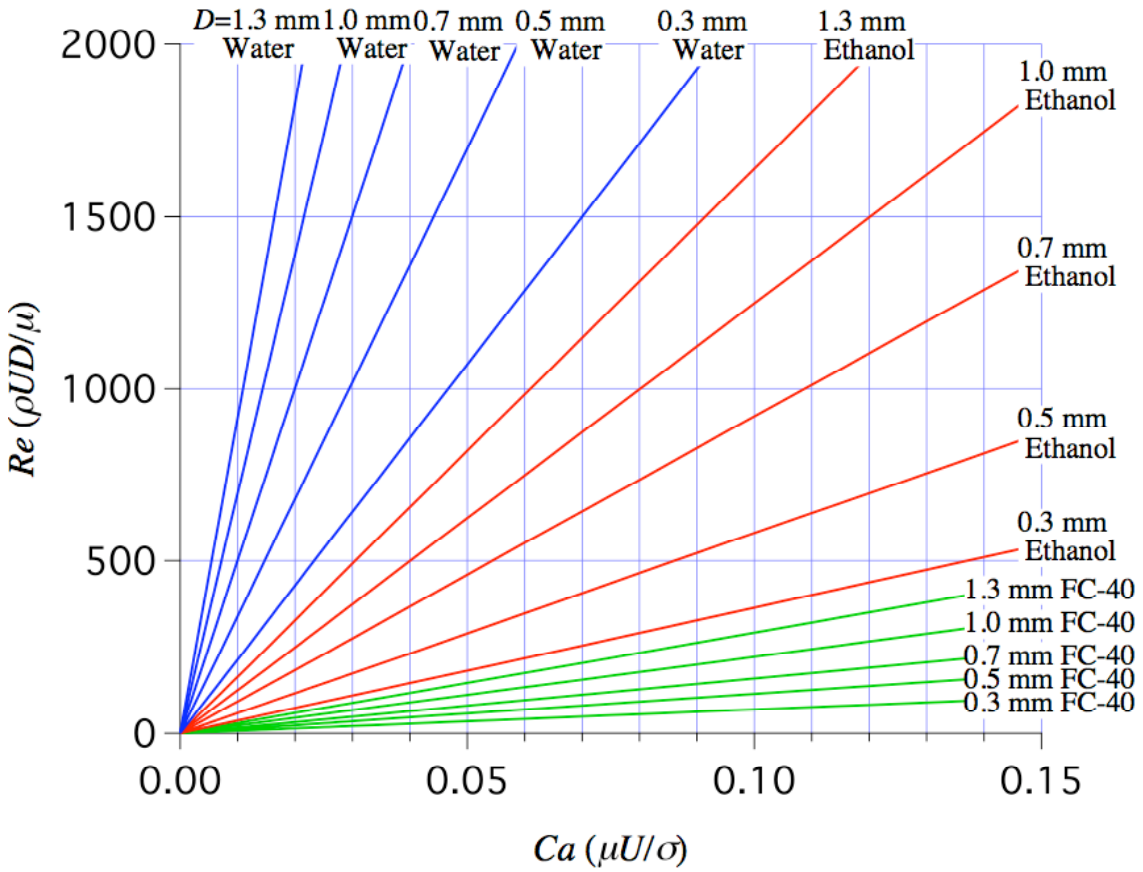
D=1.3 mm Water
1.0 mm Water
0.7 mm Water
0.5 mm Water
0.3 mm Water
1.3 mm Ethanol
1.0 mm Ethanol
0.7 mm Ethanol
0.5 mm Ethanol
0.3 mm Ethanol
1.3 mm FC-40
1.0 mm FC-40
0.7 mm FC-40
0.5 mm FC-40
0.3 mm FC-40
2000
1500
1000
500
0
0.00
0.05
0.10
0.15
Re (ρUD/μ)
Ca (μU/σ)

Fig. 8

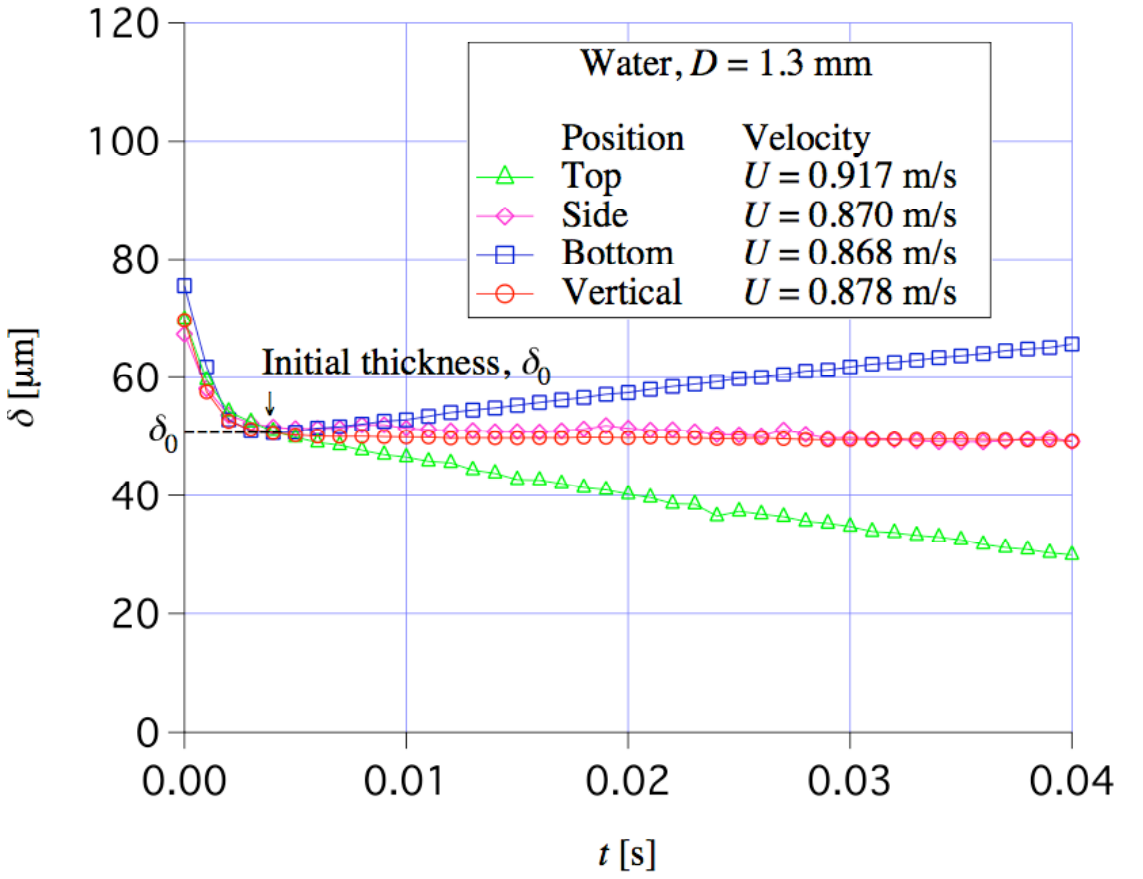
Water, D = 1.3 mm
Position
Velocity
Top
U = 0.917 m/s
Side
U = 0.870 m/s
Bottom
U = 0.868 m/s
Vertical
U = 0.878 m/s
Initial thickness, δ0
δ0
δ [μm]
t [s]
120
100
80
60
40
20
0
0.00
0.01
0.02
0.03
0.04

Fig. 9

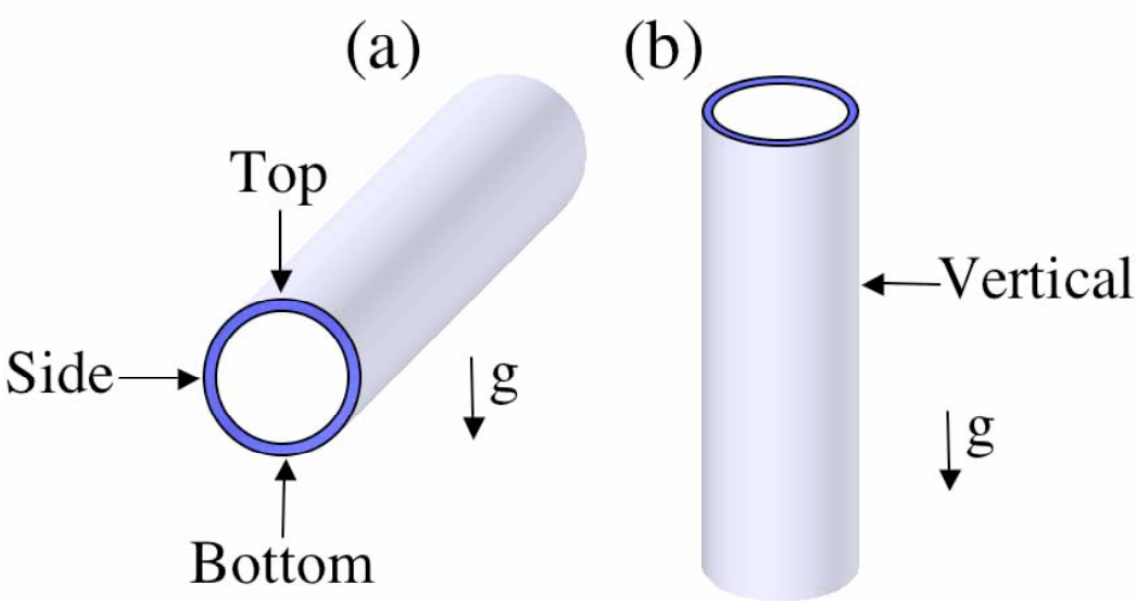
(a)
(b)
Top
Side
Bottom
g
Vertical
g

Fig. 10

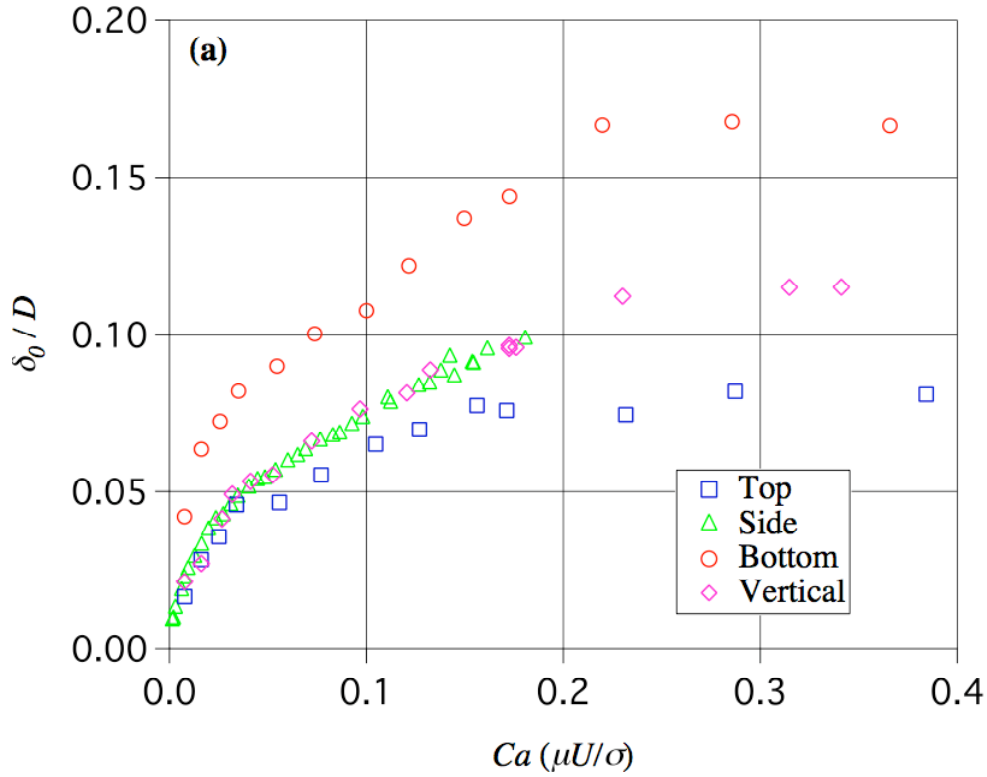
(a)
0.20
0.15
0.10
0.05
0.00
0.0
0.1
0.2
0.3
0.4
δ_0 / D
$Ca\ (\mu U/\sigma)$
Top
Side
Bottom
Vertical

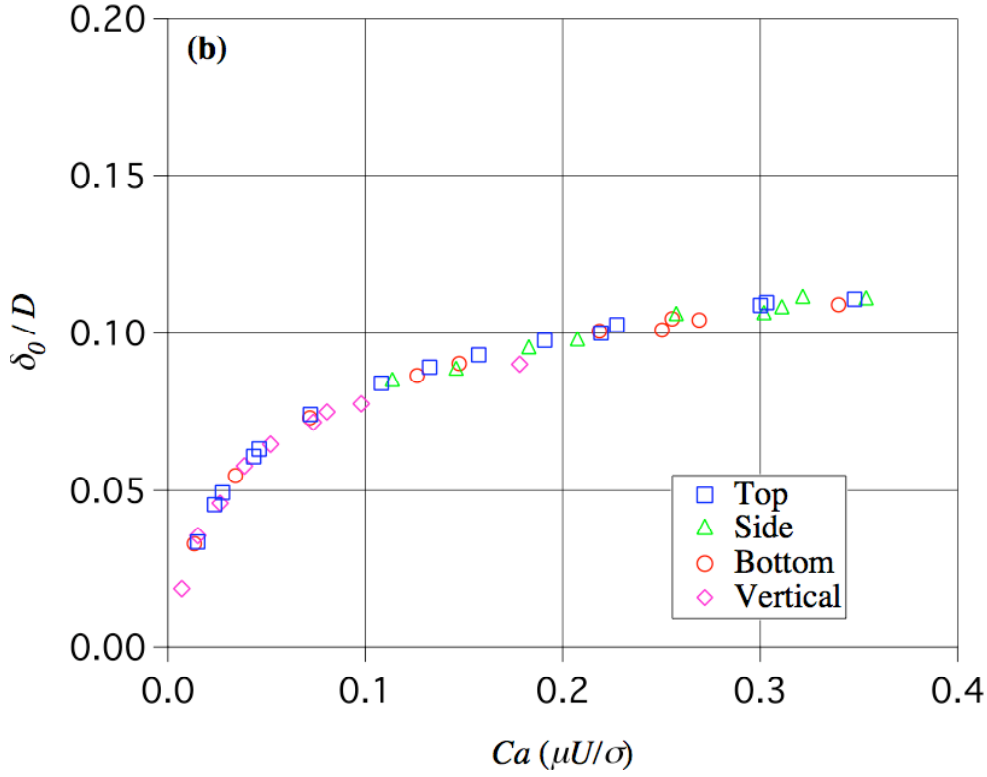
(b)
0.20
0.15
0.10
0.05
0.00
0.0
0.1
0.2
0.3
0.4
δ_0 / D
$Ca\ (\mu U/\sigma)$
Top
Side
Bottom
Vertical

Fig. 11

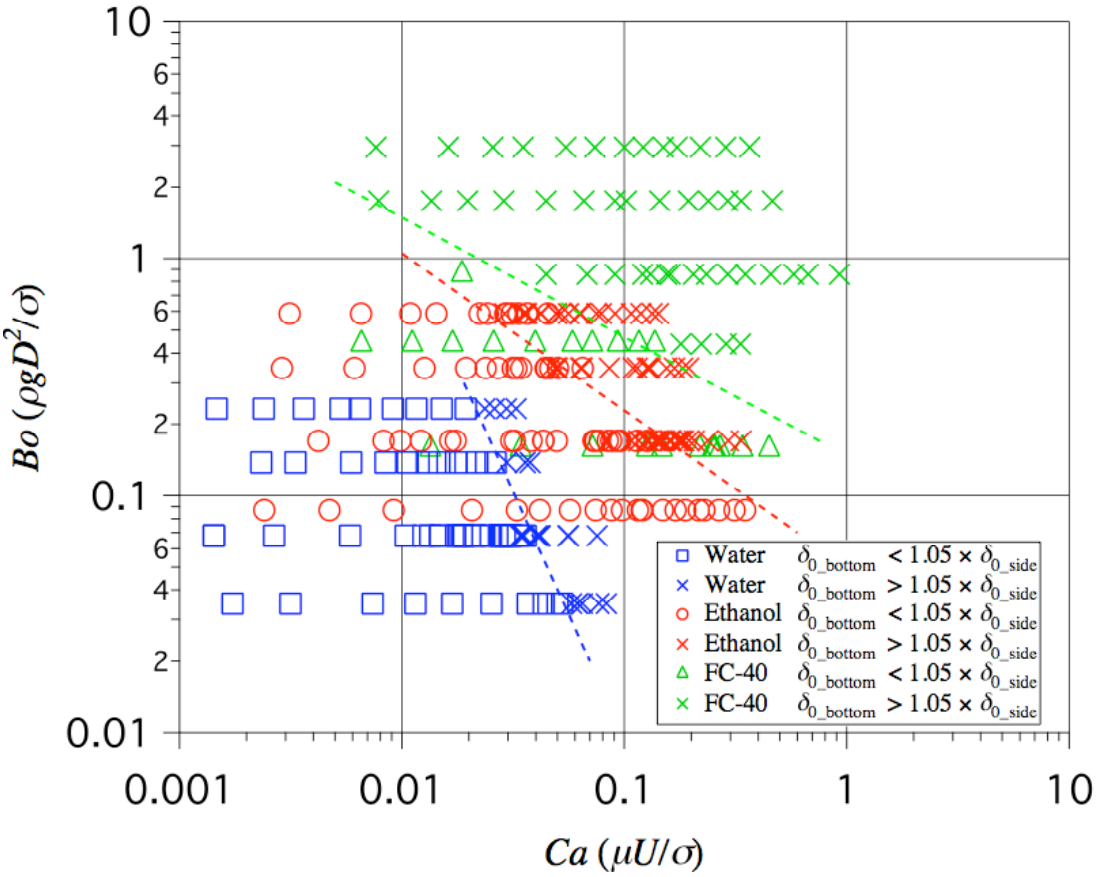
10
6
4
2
1
6
4
2
0.1
6
4
2
0.01
0.001
0.01
0.1
1
10
Bo (ρgD²/σ)
Ca (μU/σ)
Water δ0_bottom < 1.05 × δ0_side
Water δ0_bottom > 1.05 × δ0_side
Ethanol δ0_bottom < 1.05 × δ0_side
Ethanol δ0_bottom > 1.05 × δ0_side
FC-40 δ0_bottom < 1.05 × δ0_side
FC-40 δ0_bottom > 1.05 × δ0_side

Fig. 12

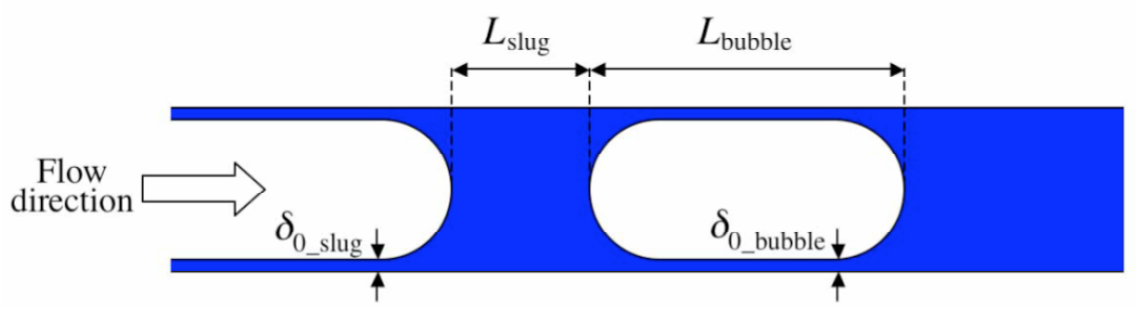
Lslug
Lbubble
Flow direction
δ0_slug
δ0_bubble

Fig. 13

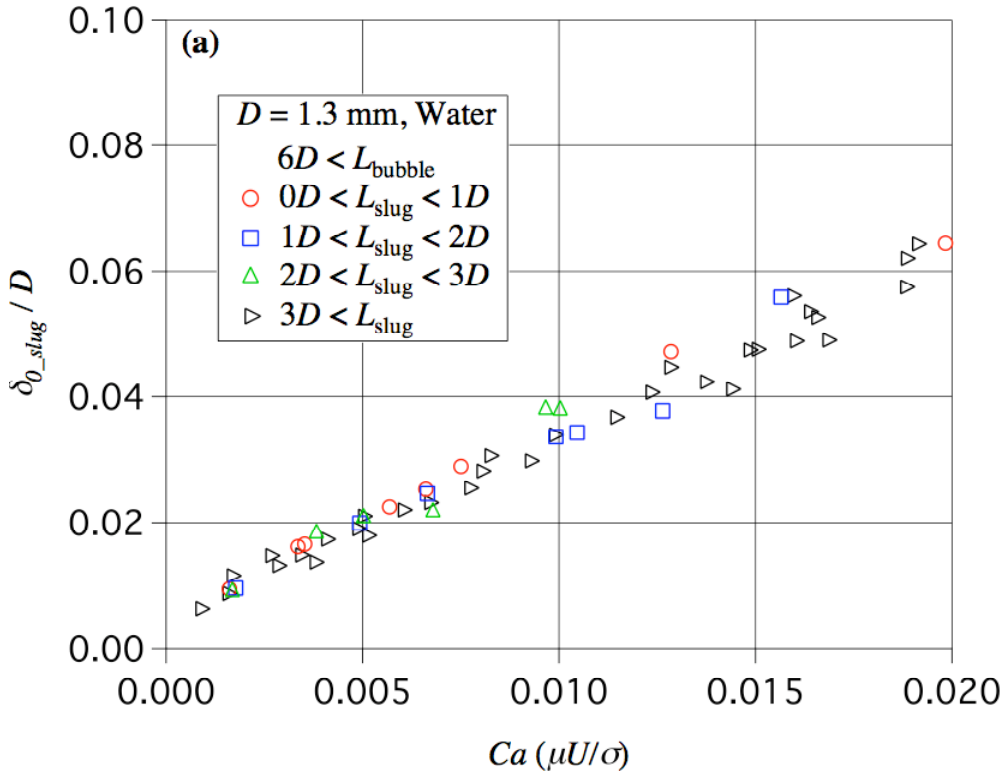
(a)
D = 1.3 mm, Water
6D < L_bubble
0D < L_slug < 1D
1D < L_slug < 2D
2D < L_slug < 3D
3D < L_slug
δ_0_slug / D
0.10
0.08
0.06
0.04
0.02
0.00
0.000
0.005
0.010
0.015
0.020
Ca (μU/σ)

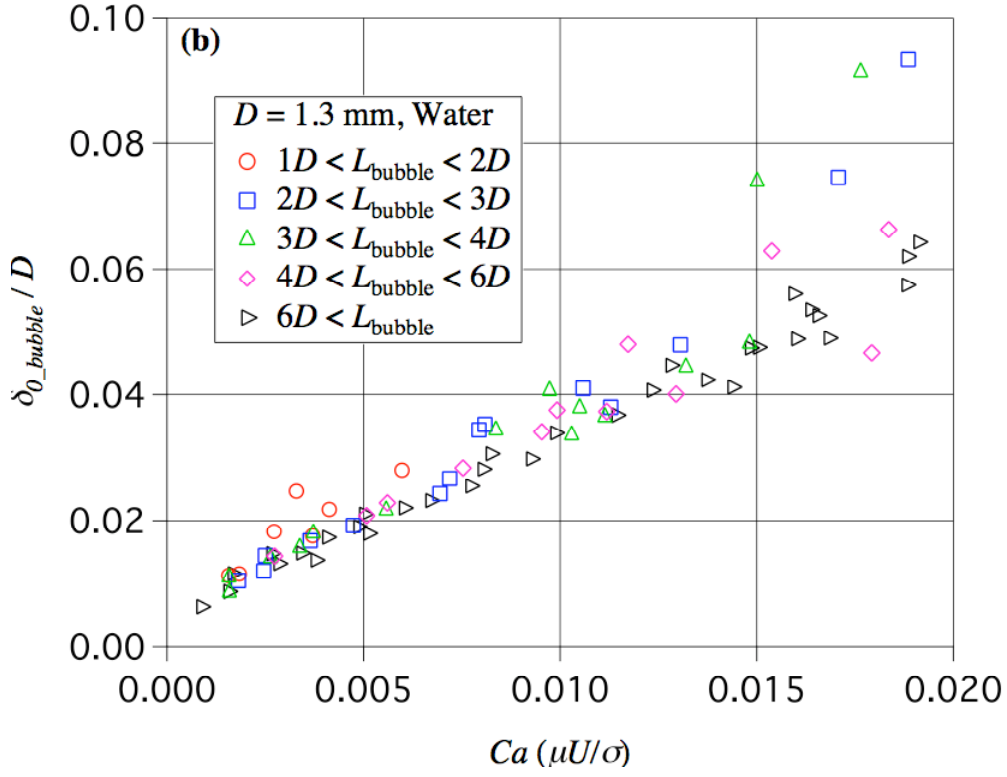
(b)
D = 1.3 mm, Water
1D < L_bubble < 2D
2D < L_bubble < 3D
3D < L_bubble < 4D
4D < L_bubble < 6D
6D < L_bubble
δ_0_bubble / D
0.10
0.08
0.06
0.04
0.02
0.00
0.000
0.005
0.010
0.015
0.020
Ca (μU/σ)

Fig. 14

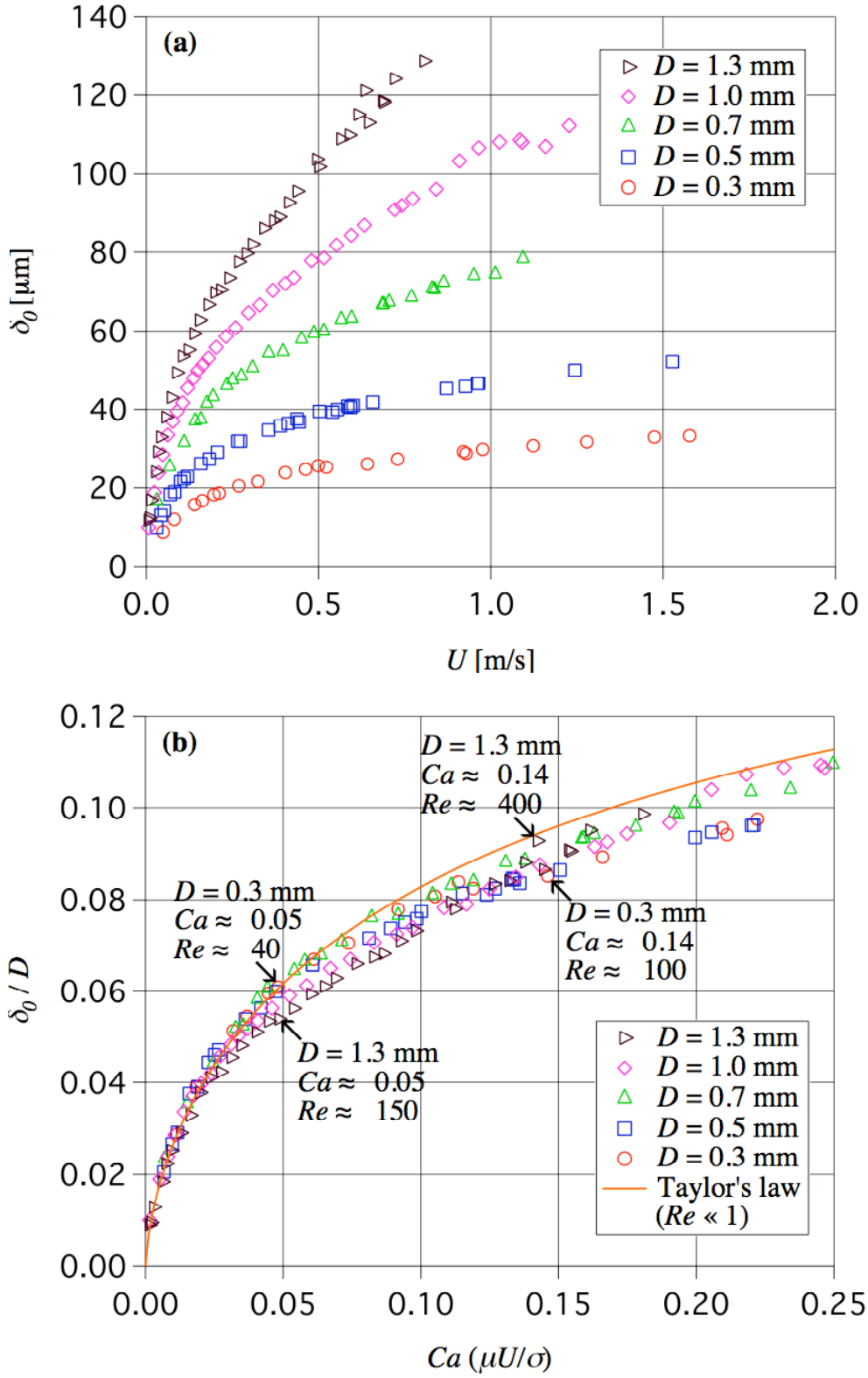
(a)
D = 1.3 mm
D = 1.0 mm
D = 0.7 mm
D = 0.5 mm
D = 0.3 mm
δ0 [μm]
U [m/s]
0
20
40
60
80
100
120
140
0.0
0.5
1.0
1.5
2.0
(b)
D = 1.3 mm
Ca ≈ 0.14
Re ≈ 400
D = 0.3 mm
Ca ≈ 0.05
Re ≈ 40
D = 0.3 mm
Ca ≈ 0.14
Re ≈ 100
D = 1.3 mm
Ca ≈ 0.05
Re ≈ 150
Taylor's law
(Re « 1)
δ0 / D
Ca (μU/σ)
0.00
0.02
0.04
0.06
0.08
0.10
0.12
0.00
0.05
0.10
0.15
0.20
0.25

Fig. 15

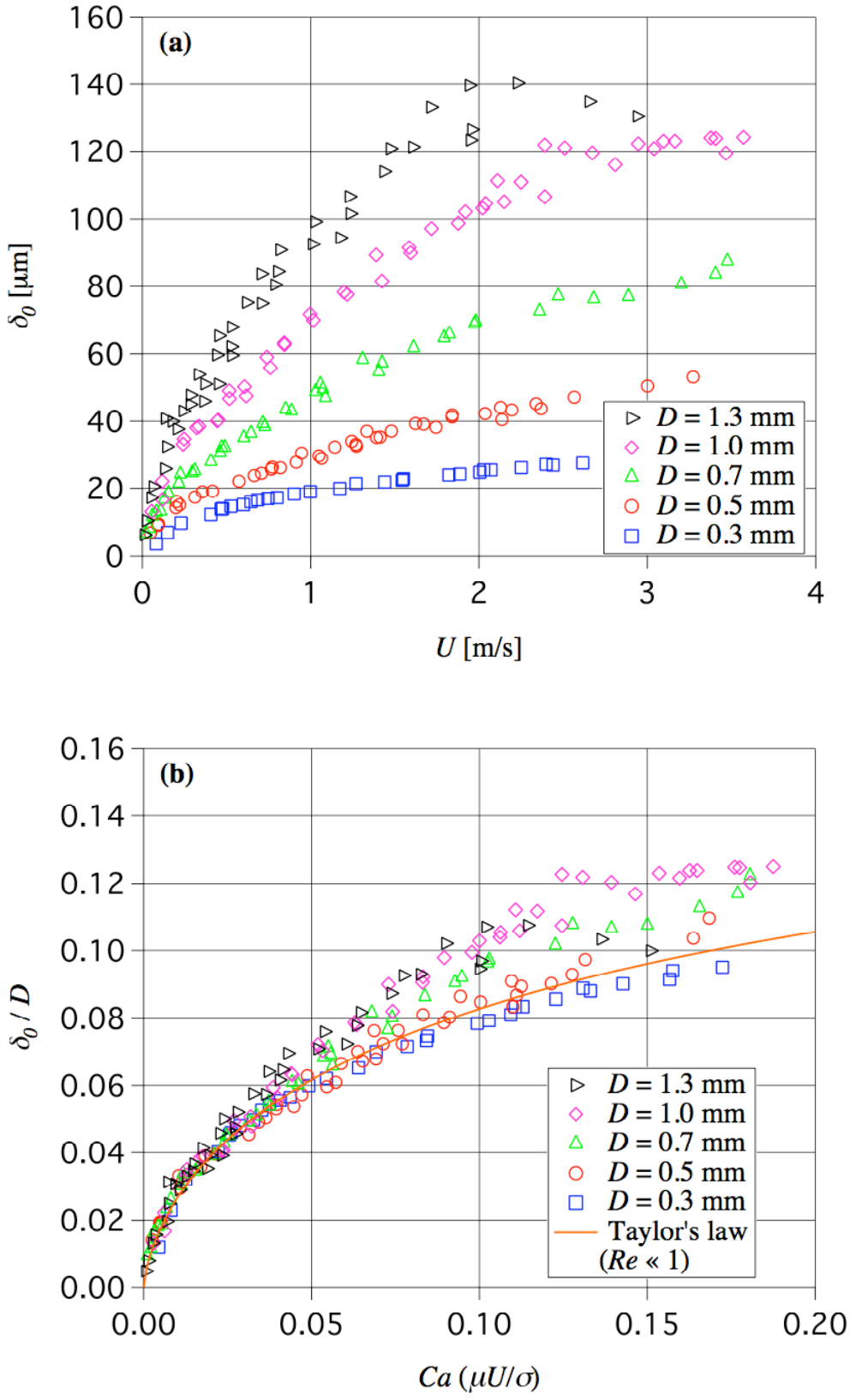
(a)
160
140
120
100
80
60
40
20
0
δ_0 [μm]
0
1
2
3
4
U [m/s]
D = 1.3 mm
D = 1.0 mm
D = 0.7 mm
D = 0.5 mm
D = 0.3 mm
(b)
0.16
0.14
0.12
0.10
0.08
0.06
0.04
0.02
0.00
δ_0 / D
0.00
0.05
0.10
0.15
0.20
Ca ($\mu U/\sigma$)
D = 1.3 mm
D = 1.0 mm
D = 0.7 mm
D = 0.5 mm
D = 0.3 mm
Taylor's law
(Re « 1)

Fig. 16

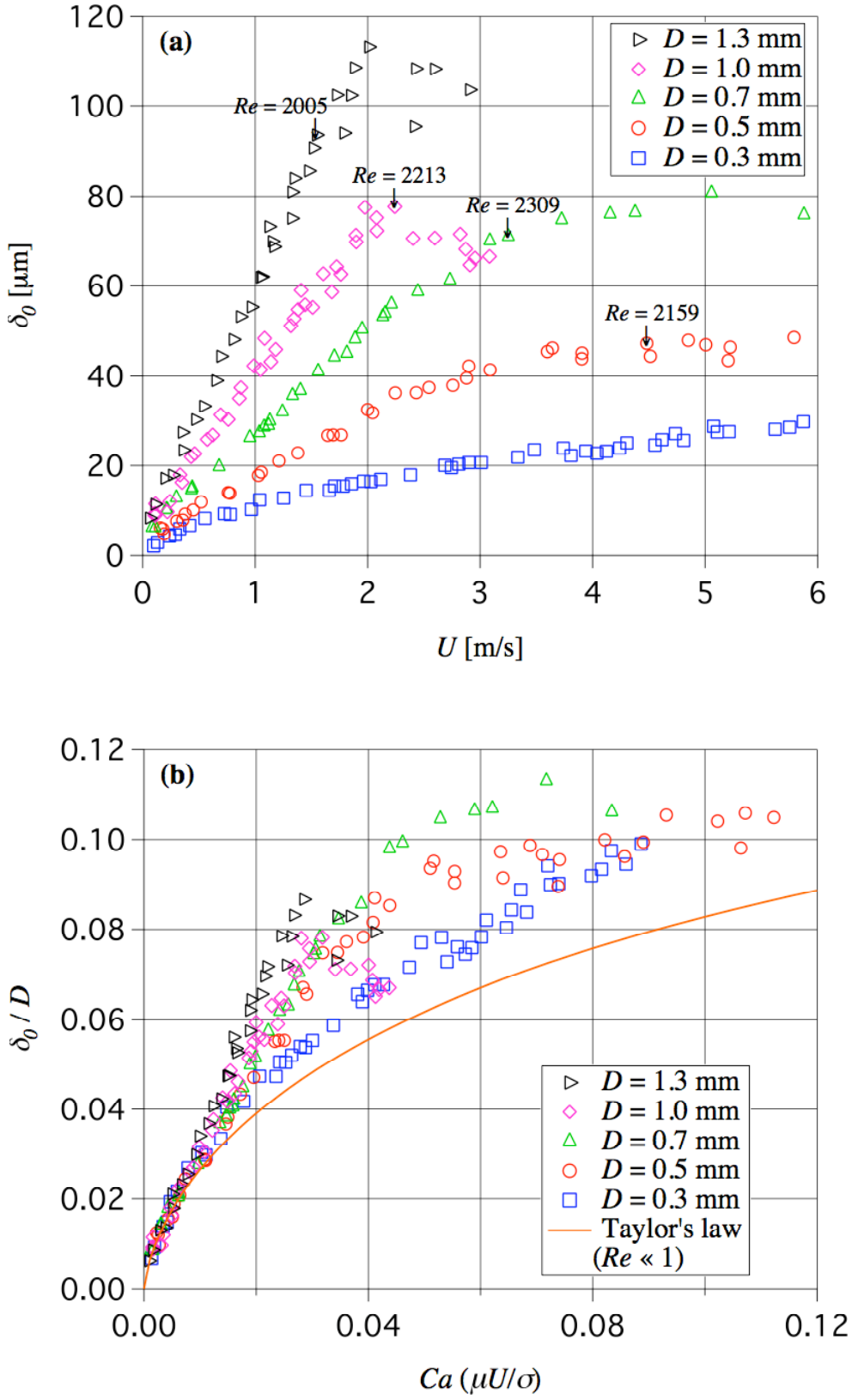
(a)
D = 1.3 mm
D = 1.0 mm
D = 0.7 mm
D = 0.5 mm
D = 0.3 mm
Re = 2005
Re = 2213
Re = 2309
Re = 2159
δ0 [μm]
U [m/s]
0
20
40
60
80
100
120
0
1
2
3
4
5
6
(b)
δ0 / D
Ca (μU/σ)
Taylor's law
(Re « 1)
0.00
0.02
0.04
0.06
0.08
0.10
0.12

Fig. 17

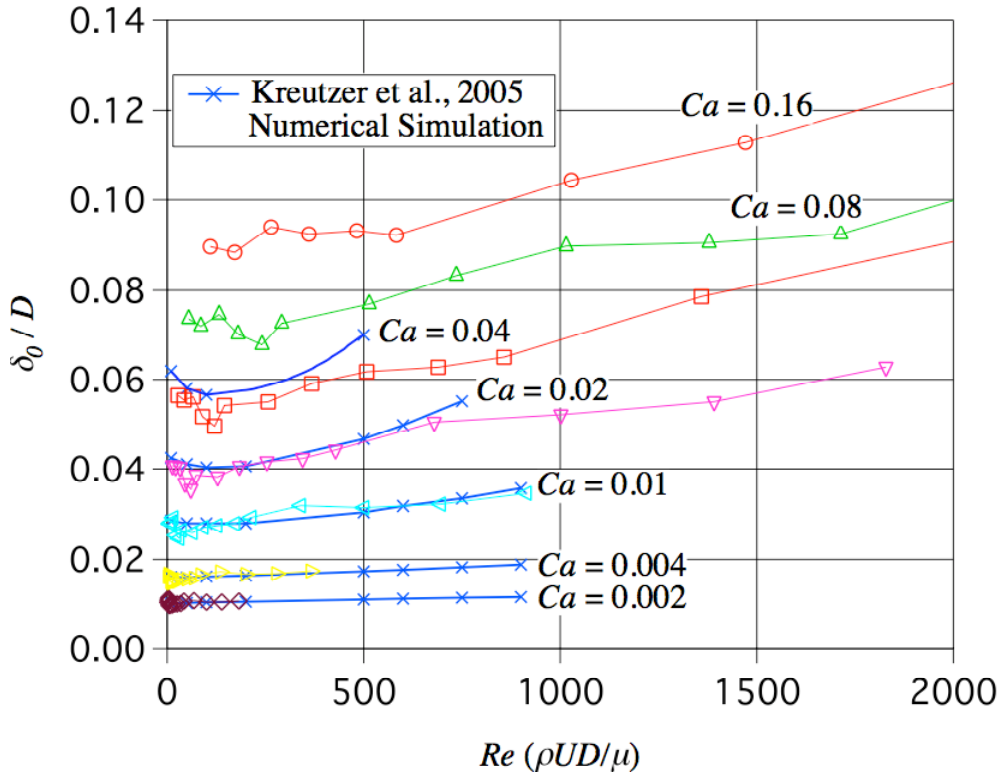
0.14
0.12
0.10
0.08
0.06
0.04
0.02
0.00
0
500
1000
1500
2000
δ_0 / D
$Re\ (\rho UD/\mu)$
Kreutzer et al., 2005
Numerical Simulation
$Ca = 0.16$
$Ca = 0.08$
$Ca = 0.04$
$Ca = 0.02$
$Ca = 0.01$
$Ca = 0.004$
$Ca = 0.002$

Fig. 18

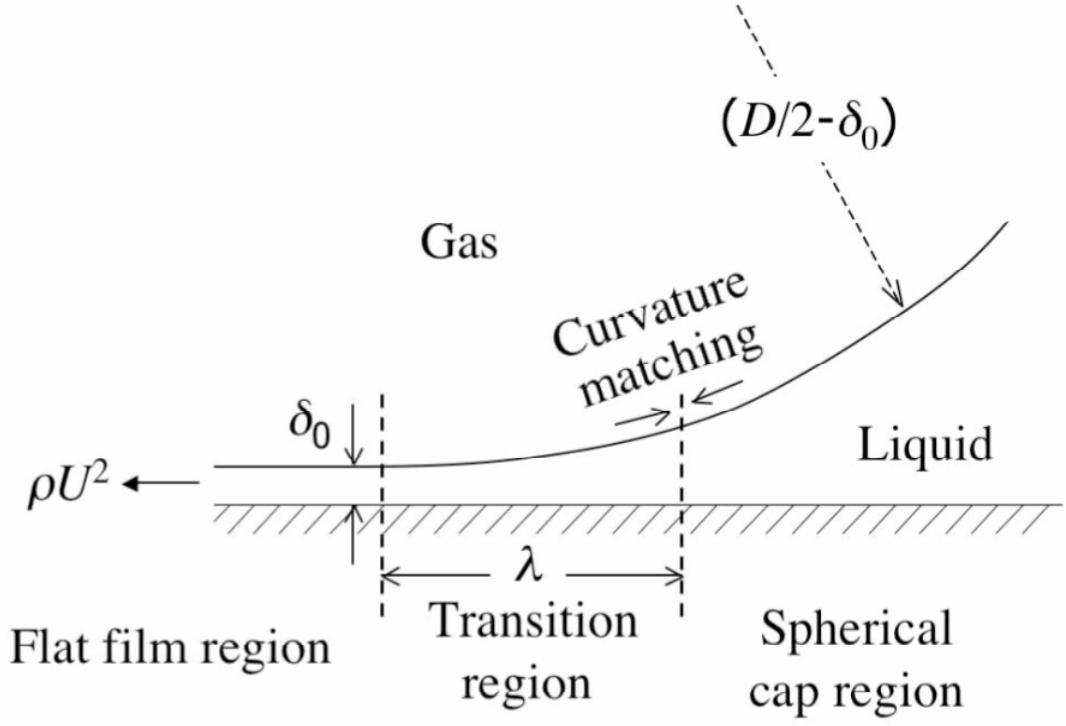
$(D/2-\delta_0)$
Gas
Curvature matching
δ_0
Liquid
ρU^2
λ
Flat film region
Transition region
Spherical cap region

Fig. 19

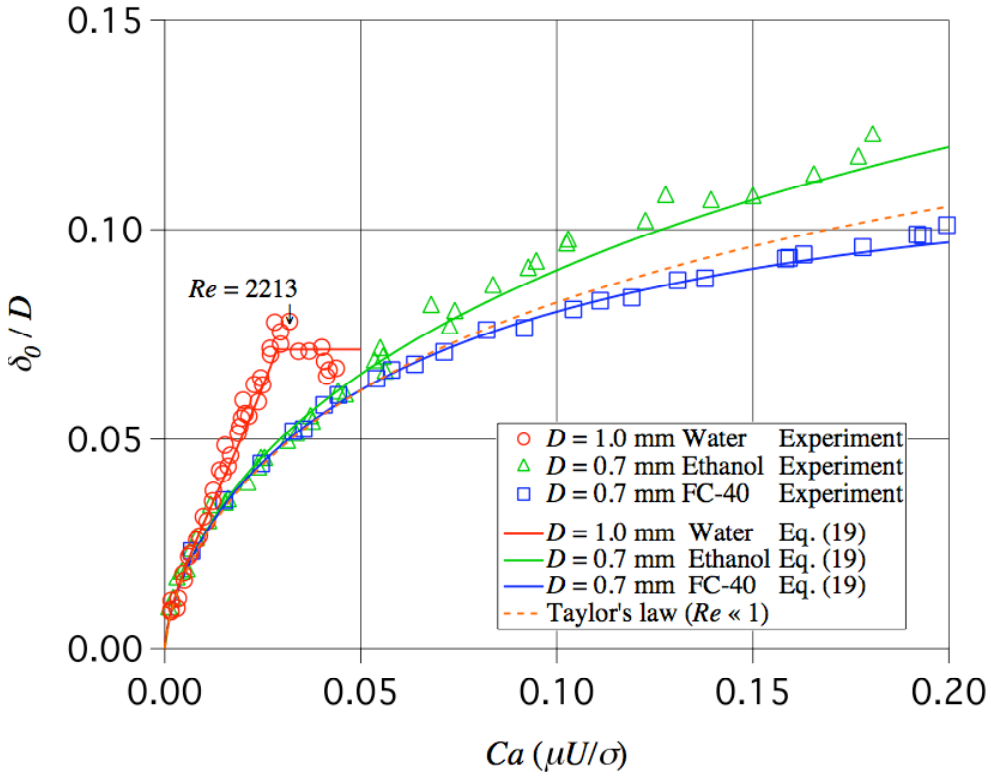
0.15
0.10
0.05
0.00
0.00
0.05
0.10
0.15
0.20
δ_0 / D
Ca ($\mu U/\sigma$)
Re = 2213
D = 1.0 mm Water Experiment
D = 0.7 mm Ethanol Experiment
D = 0.7 mm FC-40 Experiment
D = 1.0 mm Water Eq. (19)
D = 0.7 mm Ethanol Eq. (19)
D = 0.7 mm FC-40 Eq. (19)
Taylor's law (Re « 1)

Fig. 20

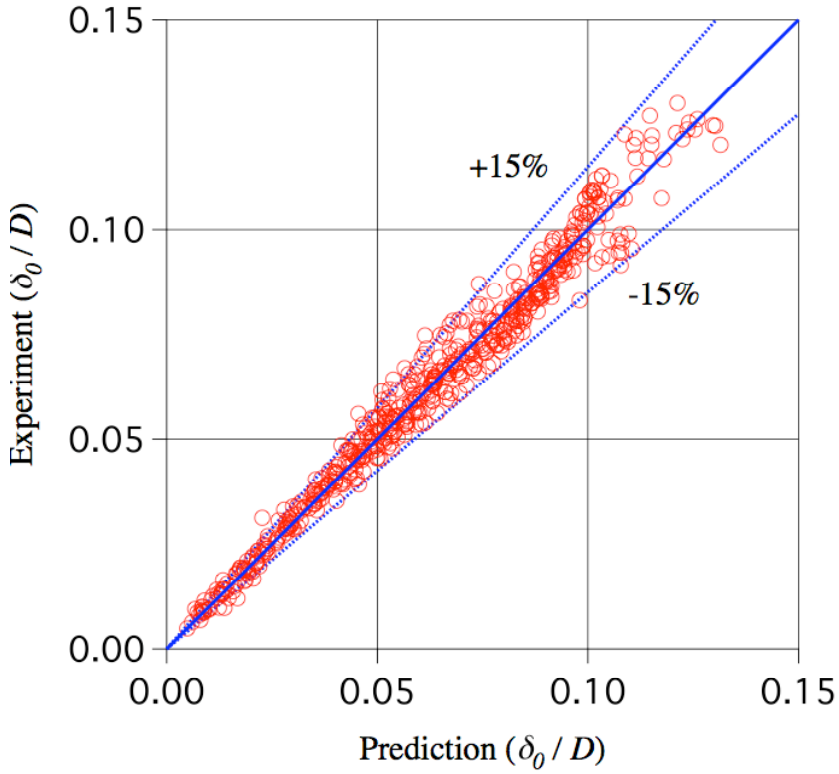
0.15
0.10
0.05
0.00
0.00
0.05
0.10
0.15
Experiment (δ_0 / D)
Prediction (δ_0 / D)
+15%
-15%

Fig. 21